Pulse Energy Optimization

in Multipass-Cavity Mode-locked Femtosecond Lasers

by

Aref MostafaZadeh

A Thesis Submitted to the
Graduate School of Engineering
In Partial Fulfillment of the Requirements for the Degree of

Master of Science
in
Electrical and Computer Engineering

Koç University
August 2010

Koç University

Graduate School of Sciences and Engineering

This is to certify that I have examined this copy of a master's thesis by

Aref Mostafazadeh

and have found that it is complete and satisfactory in all respects,
and that any and all revisions required by the final
examining committee have been made.

Committee Members:

Prof. Dr. Alphan Sennaroğlu (Advisor)

Assoc. Prof. Dr. Hakan Urey

Assoc. Prof. Dr. Alper Kiraz

Date:

August 20, 2010

Abstract

We performed a general analysis of all loss mechanisms to determine the design parameters of a Multipass-Cavity (MPC) mode-locked femtosecond Ti: Sapphire laser having the maximum output pulse energy. Advantage of the MPC design is that it allows the generation of higher output pulse energies by increasing the cavity length and consequently reducing the repetition rate. The idea of the present work is to take into account the beam clipping losses at the notches and surface of the MPC mirrors as well as the well-known reflection losses. Since losses increase with number of bounces, an optimum exists where the output pulse energy is maximized. Implementing this idea in simulations in principle can give an optimum MPC configuration with much higher pulse energy. Experimental implementation of the optimum configuration confirmed the simulation results completely. In the standard MPC configuration, maximum measured pulse energy was around 14.8nJ. In the optimum configuration, we measured 32.7nJ of pulse energy. This corresponds to an increase in the pulse energy of about 101%.

Özet

Bu tez çalışmasında, çok yansımalı kovuk (MPC) içeren, kip kilitli laserlerde ortaya çıkan tüm kayıplar hesaba katılarak, en yüksek darbe enerjisini sağlayan MPC konfigürasyonu belirlenmiştir. MPC kullanımı, laser kovuk boyunu artırarak, darbe tekrar hızının düşmesini ve daha yüksek darbe enerjilerinin elde edilmesini sağlar. Bu sistemlerin darbe enerjisi, MPC aynalarının yüzeylerinde meydana gelen yansıma kayıpları, ışınların MPC aynalarındaki yarıklardan geçerken kesilmesi ve kovuk içerisinde ışın demetlerinin ayna yüzeylerinden taşması sonucu meydana gelen kayıplardan da etkilenmektedir. Genel MPC tasarımında, yansıma kayıpları hariç diğer kayıpların sıfır olduğu varsayılır. Bu çalışmada, gerçek bir MPC laserinde karşılaşılan tüm kayıplar hesaba katılmış ve en yüksek enerjiyi verebilen konfigürasyon belirlenmiştir. Deneysel olarak kurulan optimum konfigurasyon düzeneğinden elde edilen sonuçlar, simulasyon sonuçlarının doğru olduğu göstermiştir. Standart konfigurasyonda elde edilen darbe enerjisi 14.8nJ iken, optimum konfigurasyon düzeneğinde en yüksek 32.7nJ darbe enerjisi elde edilmiştir. Bu optimizasyon neticesinde darbe enerjisi %101 oranında yükselmiştir.

Acknowledgments

I would like to thank my supervisor Prof. Dr. Alphan Sennaroğlu for his continuous support, and my brother Prof. Dr. Ali Mostafazadeh for his help in dealing with various mathematical problems, and Adnan Kurt, Hüseyin Çankaya, and Natali Çizmeciyan for valuable discussions and for their kindness and friendship. I would also like to express my gratitude to the Graduate School of Sciences and Engineering of Koç University, for providing me with the opportunity to realize my dream of engaging in scientific research, and particularly the founders and the administration of Koç University for creating and maintaining such an ideal center of excellence.

Table of Contents

List of Tables

List of Figures

Nomenclature

A	Lasing threshold coefficient
c	Speed of light in medium
d	Total effective cavity length
d_{mpc}	Length of the MPC cell
d_o	Length of the short cavity
f_{rep}	Pulse repetition rate
i	Spot index number
I	Linear luminance intensity
$I(r)$	Spatial intensity of the spots in the polar coordinates
$I(x, y)$	Spatial intensity of the spots in the Cartesian coordinates
i_L	Index number of the left adjacent spot to the notch
i_R	Index number of the right adjacent spot to the notch
L	Total cavity losses
L_{mpc}	Total MPC losses
L_o	Short cavity losses
m	m parameter of the MPC
M	Ray transfer matrix of one unit cell of the MPC
M_c	Ray transfer matrix of one unit cell of the MPC starting from the curved mirror
M_f	Ray transfer matrix of one unit cell of the MPC starting from the flat mirror
M_{mpc}	Ray transfer matrix of the MPC cell
n	n parameter of the MPC
P_{ave}	Average output power
P_{in}	Input pump power
P_{out}	Output average power
P_P	Incident pump power on the gain mediun
P_T	Transmitted power
P_{th}	Lasing threshold pump power
q	q-parameter of the beam
$q_c(i)$	q-parameter of the i^{th} spot on the MPC curved mirror
$q_f(i)$	q-parameter of the i^{th} spot on the MPC flat mirror
R	Radius of curvature
$R_{dispersio}$	Reflection coefficient of the dispersion compensation elements

R_{gti}	Reflection coefficient of the GTI mirrors
R_{mpc}	Reflection coefficient of the MPC mirrors
T	Total cavity transmission
$T_{adjacent}$	Transmission of the adjacent spots in the MPC cell
$T_{adjacent\text{-}c}$	Transmission of the adjacent spots on the MPC curved mirror
$T_{adjacent\text{-}f}$	Transmission of the adjacent spots on the MPC flat mirror
T_{center}	Transmission of the center spots in the MPC cell
$T_{center\text{-}c}$	Transmission of the center spot on the curved mirror
$T_{center\text{-}f}$	Transmission of the center spot on the flat mirror
$T_{clipping}$	Transmission due to the all clipping mechanisms in the MPC cell
T_{edge}	Transmission of a Gaussian beam through a Knife-edge
T_{in}	Transmission of the optical elements before the gain medium
T_{mpc}	Total transmission of the MPC
T_o	Transmission of the short cavity
T_{oc}	Transmission of the output coupler
$T_{reflection}$	Transmission of the MPC cell except clipping losses
$T_{surface}$	Surface transmission of the spots in the MPC cell
$T_{surface\text{-}c}$	Surface transmission of the spots on the curved mirror
$T_{surface\text{-}f}$	Surface transmission of the spots on the flat mirror
v	Gamma corrected pixel level
w	Spot size
$w_c(i)$	Spot size of the i^{th} spot on the MPC curved mirror
$w_f(i)$	Spot size of the i^{th} spot on the MPC flat mirror
w_o	Spot size of the input beam to the MPC cell
W_p	Energy per pulse (Pulse energy)
$x_c(i)$, $y_c(i)$	Coordinates of the i^{th} spot on the MPC curved mirror
$x_f(i)$, $y_f(i)$	Coordinates of the i^{th} spot on the MPC flat mirror
γ	Gamma coefficient
Δx	Distance of the Knife-edge from the spot center
Δx_c	Distance of the adjacent spots from the edge of the notch on the curved mirror
Δx_f	Distance of the adjacent spots from the edge of the notch on the flat mirror
$\Delta \rho_c$	Difference in the radius of the MPC mirror and the spot pattern on the curved mirror
$\Delta \rho_f$	Difference in the radius of the MPC mirror and the spot pattern on the flat mirror
η	Slope efficiency
η_a	Fractional pump power absorption
η_{klm}	Slope efficiency of the extended cavity in KLM operation

η_{short}	Slope efficiency of the short cavity
θ	Angular advance angle of the MPC
$\theta(i)$	Angle of the i^{th} spot on the MPC mirrors
λ	Wavelength
λ_P	Pump wavelength
λ_L	Lasing wavelength
ρ_{mpc}	Radius of the MPC mirrors
$\rho_{pat\text{-}c}$	Radius of the spot pattern on the MPC curved mirror
$\rho_{pat\text{-}f}$	Radius of the spot pattern on the MPC flat mirror

1 Introduction

Femtosecond solid-state lasers have many applications in a variety of fields such as biomedical imaging [1], spectroscopy [2, 3], high harmonic generation [4, 5], and so on. From a commercial point of view, the most expensive part of such systems is the pump laser whose price is directly related to its output power. Introducing methods to design low cost systems that can attain higher pulse energies with low power pump lasers is valuable. Tight focusing cavity design is one of the methods of lowering the required pump power for achieving low threshold mode-locked operation [6]. However, for most applications, we need also high pulse energy and peak powers. One way of doing this is to extend the cavity length. Since the pulse energy is related to the cavity length in mode-locked operation, extending the cavity will reduce the pulse repetition rate. Furthermore, because increasing the cavity length has no major effect on losses, the average power will remain roughly unchanged while the pulse energy will increase to the same extent as the length of the cavity. This also requires additional dispersion to balance the nonlinearity induced by the higher pulse energies. For example, if we want to reduce the repetition rate from 200MHz to 10MHz, we must increase the cavity length from 1m to 20m. However, for most applications constructing such a long cavity is not practical.

A smart solution to this problem involves using a Herriot-type multipass cavity (MPC) that extends the cavity length while maintaining the compactness of the system by using multiple reflections of the laser beam inside the multipass cavity cell. This method was proposed for the first time by Cho et al. in 1999 [7]. They increased the cavity length of a mode-locked Ti: Sapphire laser that generated 16.5fs pulses with a peak power of 0.7MW at a pulse repetition of 15MHz.

The multipass cavity consists of two highly reflecting mirrors and a mechanism to inject and extract the beam. [8]. The main disadvantage of the multipass cavities is the increased total losses of the cavity due to the high number of reflections inside the cell. Additional MPC losses can reduce the average output power. In this thesis work, we analyzed all loss mechanisms of MPC cell in a femtosecond laser by simulating all possible design configurations. In particular, we considered possible clipping and reflection losses. As a result of these simulations we demonstrated the practically achievable optimum configuration that produces the highest possible output pulse energy.

1.1 Mode-locked Femtosecond Lasers

In general, the gain media for the ultra-short femtosecond lasers are broadband solid-state media that allow amplification over a wide spectral region. These gain media are usually insulating crystals or glasses doped with rare earth or transition metal ions. Different lasing wavelengths from ultraviolet to infrared are possible using various ion-host combinations [9].

The pulsewidth of the mode-locked laser depends on the bandwidth of the gain medium, reflection bandwidth of the cavity optics, cavity dispersion and spectral bandwidth of dispersive elements. Typical pulsewidths are in the range of picoseconds (10^{-12}) to femtoseconds (10^{-15}). [10, 11, 12]

1.1.1 Mode-locking

In a laser resonator there are many equally spaced longitudinal modes. In mode-locked operation, all of these longitudinal modes are forced to oscillate in phase. This produces a periodic pulse train whose repetition rate is equal to the frequency spacing between longitudinal modes, namely

$$f_{rep} = \frac{c}{2d}. \tag{1.1}$$

Here f_{rep} is the repetition rate, d is the optical length of resonator’s effective length, and c is the speed of light [13].

Mode-locking operation can be classified into two regimes, active and passive mode-locking. In both of these methods, there is a gain/loss modulation mechanism. In active mode-locking, a fast acousto-optic device operating at a frequency close to the repetition rate of the cavity initiates the generation of the ultra short pulses. In passive mode-locking, an intensity-dependent property acts as the gain/loss switching mechanism. In this case, high intensity fluctuations experience higher optical gain inside the resonator. This behavior forces the modes to oscillate in phase to generate high-intensity pulses. Passive mode-locking can be achieved in two different ways: 1) Using SEemiconductor Saturable Absorber Mirrors (SESAMs); 2) Using non-linear Kerr effect. The latter is also known as Kerr Lens Mode-locking (KLM) which we use in our experimental setup.

1.1.2 Kerr-Lens Mode-locking

The Kerr effect is a change in refractive index of the material due to an externally applied electric field or electric field component of the incident optical beam. The amount of the Kerr effect for different materials depends on their Kerr constant. Since the Kerr effect is a very weak effect, it can only be observed with very high electric fields or very high optical intensities such as in lasers. This effect was discovered by Scottish physicist John Kerr in 1875 [14].

As an interesting result of this effect inside an optical crystal, a high intensity incident optical beam can cause a spatial change of the refractive index. This acts as a self-focusing lens inside the crystal. If the crystal is a gain medium of a laser resonator, this self-focusing causes to shift the laser's beam waist to a new location. With careful alignment of the cavity, it is possible to improve the overlap between the pump and laser beams to increase the gain. This situation favors the oscillation of the mode-locked pulses with higher peak power as opposed to the constant (CW) output. KLM effect is schematically shown in Figure 1-1 [15].

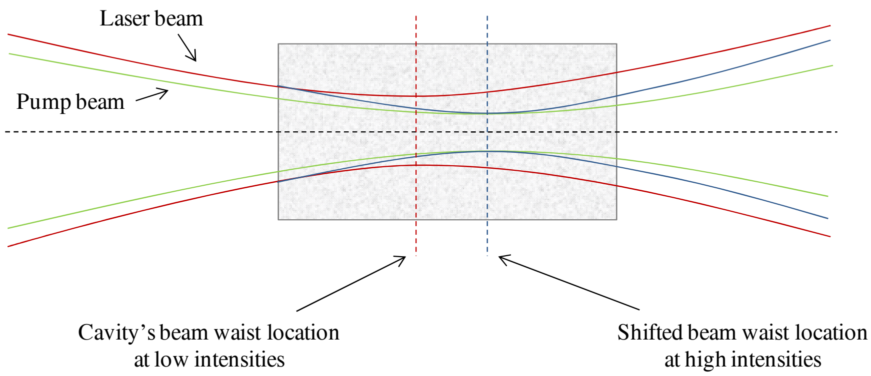

Figure 1-1 - Kerr lens self focusing effect inside the lasing crystal

1.2 Pulse Energy in Mode-locking Operation

The average output power of the laser P_{ave} and the pulse energy W_p in mode-locked operation are related according to

$$W_p = \frac{P_{ave}}{f_{rep}}. \tag{1.2}$$

In view of Equations 1.1 and 1.2, the pulse energy is given by

$$W_p = \frac{2P_{ave}}{c} d. \tag{1.3}$$

According to Equation 1.3, for a constant average output power, the pulse energy is directly related to the cavity length. Therefore, if we extend the cavity, the pulse energy increases proportionally. In practice, extending the cavity using MPCs will introduce additional losses to the system. These losses will reduce the output average power. In most cases, however, this is negligible in comparison with the increase in pulse energy. An in-depth analysis of these losses can be helpful in designing the optimum MPC configuration for obtaining the highest possible pulse energy.

2 Multipass-Cavities

Paraxial ray analysis in periodic focusing wave-guides was first applied to electron beams by Pierce in 1954 [16]. Extension of this idea to optical beams was first investigated by Herriot et al. in 1964 [17]. Integration of the Herriot type multi-pass cavities with mode-locked femtosecond lasers for achieving higher pulse energies was first done by Cho et al. in 1999 [18].

In general, MPCs consist of two main mirrors and a mechanism for injecting and extracting the beam. To preserve the stability of the system, at least one of the mirrors must be curved. Therefore, there are two possible MPC designs: flat-curved and curved-curved designs. There are also two different methods of injecting and extracting the beam, namely using pick off mirrors or using notches on the MPC mirrors. Figure 2-1 shows a 3D sketch of a MPC cell with notches.

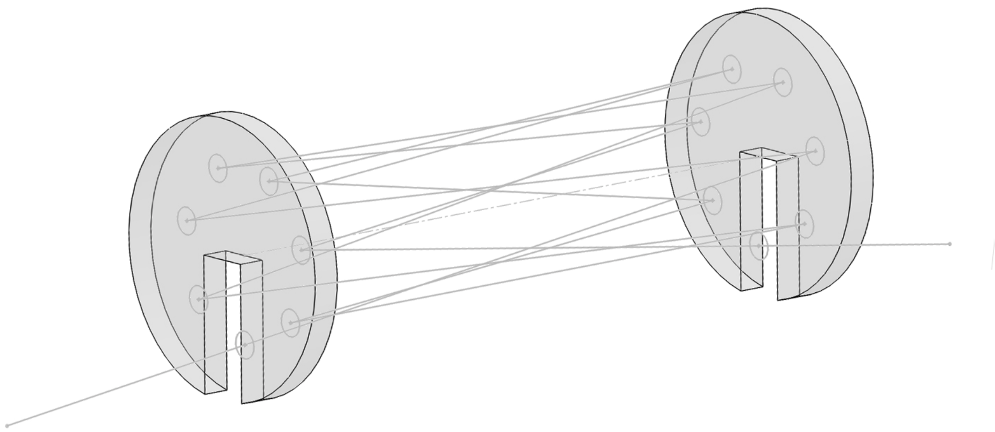

Figure 2-1 - 3D Sketch of a MPC cell with notches

2.1 Q-preserving Property

In mode-locked lasers, any change in the cavity dimensions results in a change in the operational point of the laser. This is very important because the mode-locked operation is possible only in very small intervals of the cavity's stable region. Using Herriot type multipass cavities for extending the cavity length, one can design an MPC in such a way that the incoming beam parameter is left unchanged after it traverses its path through the MPC and returns to the short cavity. This is called a q-preserving MPC. It keeps the operating point of the mode-locked laser unchanged [19].

2.1.1 Paraxial Optics

By definition, paraxial rays are rays whose angular deviation from the optical axis is small enough so that the sine and tangent of the angle can be approximated by the angle itself. In paraxial optics, a ray can be described by its distance and slope relative to optical axis. These parameters are represented as a 2×1 column vector

$$\vec{r} = \begin{bmatrix} x \\ x' \end{bmatrix}. \tag{2.1}$$

Here x is the distance from the optical axis and x' is the slope of the ray [20] (see Figure 2-2).

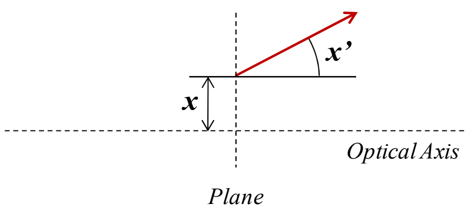

Figure 2-2 - Distance and angle of inclination describing a paraxial ray

In an optical system, if we use $\vec{r}_{in}$ and $\vec{r}_{out}$ to denote the incoming and outgoing rays (see Figure 2-3), then the relation between the input and output can be expressed by

$$\vec{r}_{out} = \begin{bmatrix} A & B \\ C & D \end{bmatrix} \cdot \vec{r}_{in}, \tag{2.2}$$

where, the 2×2 ABCD matrix is the ray transfer matrix of the optical system.

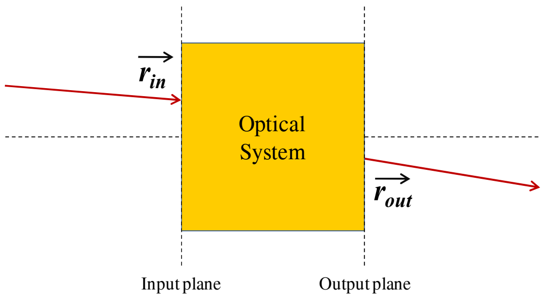

Figure 2-3 - An optical system with input and output rays

2.1.2 Q-parameter of Gaussian Beams

For a Gaussian beam, the q-parameter is a complex number involving the spot size and wave front curvature of the beam. It is defined by [21]

$$\frac{1}{q} = \frac{1}{R} + j\frac{-\lambda}{\pi w^2}, \tag{2.3}$$

where R is the radius of curvature of the wavefront, λ is the wavelength of the beam in the medium, and w is the spot size. In an optical system whose input is a Gaussian beam with q-parameter q_{in}, the output q-parameter q_{out} can be described using ABCD ray transfer matrix [22]

$$q_{out} = \frac{Aq_{in} + B}{Cq_{in} + D}. \tag{2.4}$$

2.1.3 Q-Preserving Condition in MPCs

To obtain an analytic solution for the q-preserving condition, first we must write the ray transfer matrix of the MPC cell. Figure 2-4 and 2-5 show the general curved-curved MPC design and its lens equivalent model.

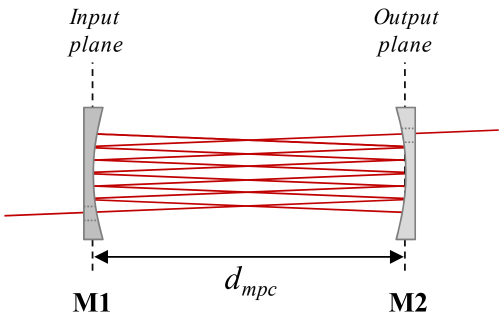

Figure 2-4 - Curved-curved MPC design

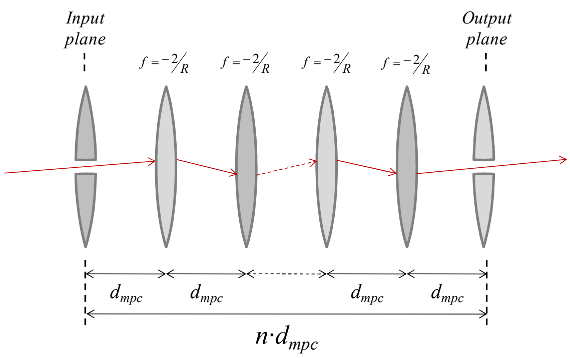

Figure 2-5- Lens equivalent model for curved-curved MPC design

As shown in these pictures, the ray transfer matrix of the MPC can be expressed in terms of its unit cell matrices. If we denote the ray transfer matrix of a single round trip of the MPC by M and the number of total round trips inside the MPC by n, the total ray transfer matrix is given by

$$M_{mpc} = M^{n}. \tag{2.5}$$

For an MPC to be Q-preserving, the q-parameter of the returning beam q_{out} must be exactly equal to the q-parameter of the incoming beam q_{in};

$$q_{out} = q_{in}. \tag{2.6}$$

Now according to Equation 2.4, M_{mpc} must be equal to ±I, where I is the unity matrix. In general, we have

$$M_{mpc} = M^n = (-1)^m I, \tag{2.7}$$

where m is an integer.

Analytically it can be shown that the general rule for an MPC to be q-preserving is,

$$m\pi = n\theta. \tag{2.8}$$

Here m is the number of semi-circles that the bouncing beam traverses on each mirror in full n round trips before the q parameter is transformed back to its initial value, and θ is the angular advance of the beam inside the MPC for each reflection [23]. Figure 2-6 shows the angle θ for two different MPC configurations with m=2 and m=4.

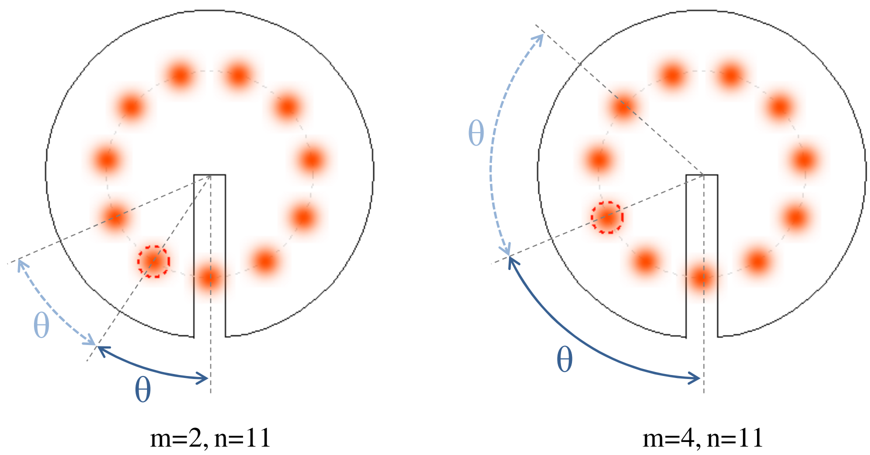

Figure 2-6 - The angular advance (θ) in two different configuraitons.[1]

[1] Dashed circles indicate the first spot on the mirrors.

Now, when m is even, the bouncing beam traces out an integer number of full circular trajectories after n roundtrips. This corresponds to the case $M_{mpc}=I$. When m is odd, the beam undergoes an integer number of half circular trajectories, and $M_{mpc}= -I$. Herriot identified the q-preserving case with even m value as reentrant condition. In practice for even m values, the mirror notches will be in the same direction but for odd m values the notches will be in the opposite direction. Figure 2-7 shows the spot pattern for various m values in a flat-curved MPC. In this flat-curved design, input beam enters form the notch of the curved mirror and goes out through the notch of the flat mirror.

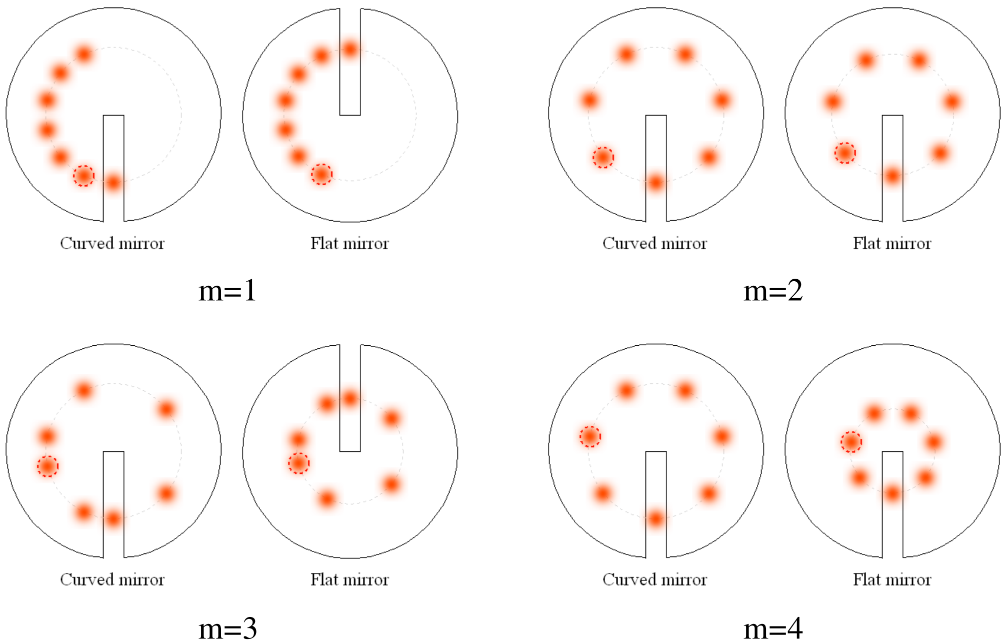

Figure 2-7 - Spot Patterns for various m values in a flat-curved MPC (n=7) [1, 2]

[1] In this Figure we considered fixed spot sizes to show the location of the spots only.
[2] The pattern radius on the flat mirror has a fixed ratio to the pattern radius of the curved mirror, which depends on MPC paramteres. See 3.1.5. for details.

2.2 Realizable Configurations in Flat-Curved MPC Design

For the flat-curved MPC design, there are two constraints for configurations that can be implemented in practice. First, the angular advance θ for flat-curved MPC must be smaller than or equal to π [24].[1] Using this constraint and the principal q-preserving condition mπ = nθ, we have

$$\theta \leq \pi \xrightarrow{m\pi = n\theta} m \leq n. \tag{2.9}$$

The other constraint for m and n combination results from the overlapping of the spots in multiple roundtrips. For example, consider n=8 and m=4. In this configuration, the angular advance θ is π/2. In this case, the fourth spot will be overlapped on the notch, the beam will go out, and the remaining bounces will not be completed. This condition can occur only in multiple roundtrips on mirrors (m>2). The mathematical constraint for preventing such combinations is,

$$n \text{ and } {}^{m}\!/_{2} \text{ must be relatively prime to each other.} \tag{2.10}$$

This eliminates the m=n condition of the first constraint. Then the first constraint must be also adapted as,

$$m < n \tag{2.11}$$

Table 2-1 shows all of the realizable configurations for even m values[2] between 2 and 10 and n up to 20.[3]

[1] The constraint for curved-curved design is θ ≤ 2π.
[2] The various m values in all graphs are color coded from dark brown to orange corresponding to m=2, 4, 6, 8 and 10.
[3] The algorithm for finding the implementable configurations is discussed in 3.3.6.

m \ n	1	2	3	4	5	6	7	8	9	10	11	12	13	14	15	16	17	18	19	20
2	-	-	●	●	●	●	●	●	●	●	●	●	●	●	●	●	●	●	●	●
4	-	-	-	-	●	×	●	×	●	×	●	×	●	×	●	×	●	×	●	×
6	-	-	-	-	-	-	●	●	×	●	●	×	●	●	×	●	●	×	●	●
8	-	-	-	-	-	-	-	-	●	×	●	×	●	×	●	×	●	×	●	×
10	-	-	-	-	-	-	-	-	-	-	●	●	●	●	×	●	●	●	●	×

Table 2-1 - Realizable configurations for even m values

2.3 Compensated MPCs

In order for the MPC to be q-preserving, n full roundtrips must be completed in m semicircles. However it is not possible to extract the last roundtrip using a notch on the mirror. In this case, a maximum of n-1 complete roundtrips can be completed. Therefore, one additional roundtrip must be added to make the MPC q-preserving. Figure 2-9 shows the additional roundtrip after extracting from the MPC cell.

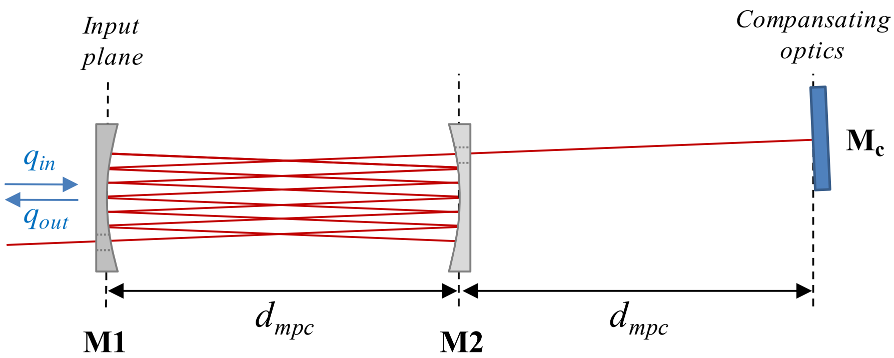

Figure 2-8 - Compansated non-q-preserving MPC setup

In this case, using ray transfer matrices, we can calculate the compensating optics for the MPC to be q-preserving. For the specific flat-curved design (M1 is a curved mirror with radius of curvature of R and M2 is a flat mirror) the compensating optic will be a curved mirror with a radius of curvature of R/2 [25].

3 Simulation and Analysis of Flat-Curved MPC

The multi-pass cavity (MPC) design that we used for extending Ti: Sapphire laser cavity is shown in Figure 3-1. The MPC consists of a curved mirror with a radius of curvature of R and a flat mirror, both with notches, and a third curved end mirror with a radius of curvature of R/2. The end highly reflecting mirror is at a distance of d_{mpc} from the reference plane Z_f at the flat mirror.

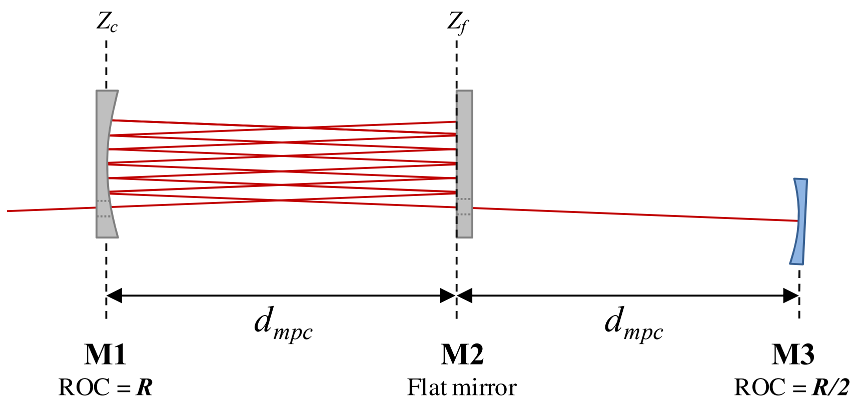

Figure 3-1 - Flat-curved MPC cell

Figure 3-2 shows the lens equivalent model of the MPC. Here Z_c is the reference plane of curved mirror (which is the input plane) and Z_f is the reference plane of the flat mirror.

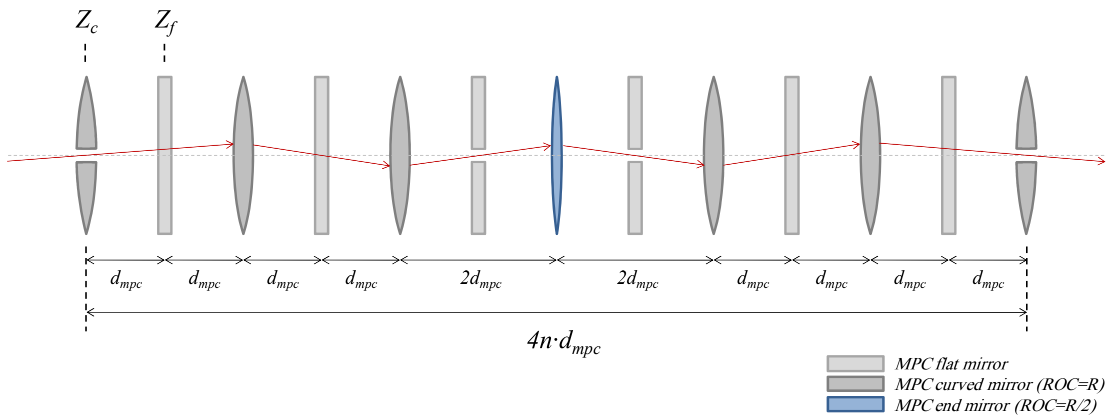

Figure 3-2 - Lens equivalent model of flat-curved MPC design

As shown in Figure 3-2, entering beam bounces n roundtrips between the MPC mirrors and goes out from the flat mirror's notch, and then it reflects back from the end mirror, bounces n roundtrips again between MPC mirrors, and finally goes out exactly from the initial input point and on the same optical path. In this case, total cavity extension is $4n \cdot d_{mpc}$. Figure 3-3 shows the implemented MPC cell in our experimental setup.

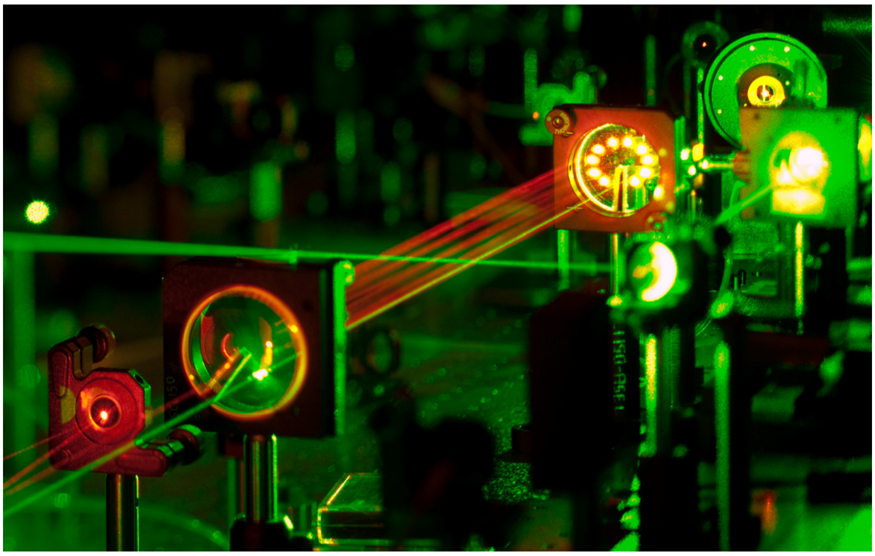

Figure 3-3 - Implemented MPC cell in our experimental setup.

3.1 Modeling and Simulation of the MPC

For modeling of the optical beams inside the MPC, we need to calculate the dimensions and the locations of the spots on the MPC mirrors. For calculating the spot sizes, we first propagate the beams inside the MPC cell using the ray transfer method. Using the resulting complex beam parameters, the spot sizes can be calculated. Finally, we calculate the spot locations on the MPC mirrors by using a simple geometry.

3.1.1 Propagation of the Beams inside the MPC

Due to the q-preserving property of the MPC, we need to calculate the propagation of the beams only in one direction. In the reverse direction, the spots are identical but in reverse order. We use two different unit cell transfer matrices, one starting from the curved mirror surface Z_c and the other from the flat mirror surface Z_f. Detailed lens equivalent sketch in Figure 3-3 shows these unit cells.

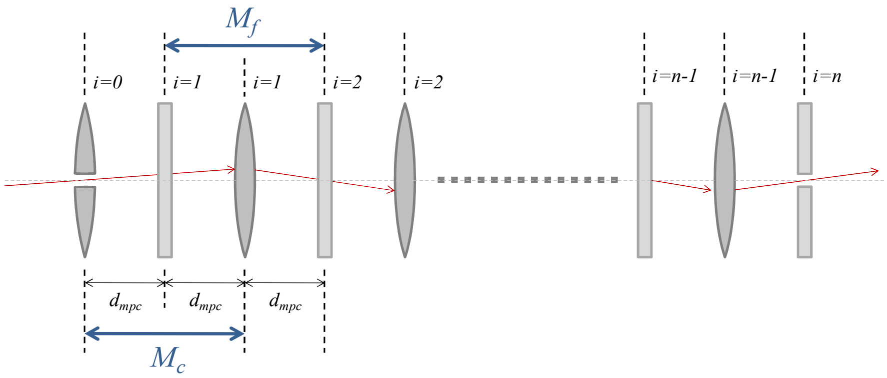

Figure 3-4 - Beam propagation in MPC

The first unit cell starting from the curved mirror plane has the ray transfer matrix M_c given by

$$M_c = \begin{bmatrix} 1 & 0 \\ -2/R & 1 \end{bmatrix} \begin{bmatrix} 1 & d_{mpc} \\ 0 & 1 \end{bmatrix} \begin{bmatrix} 1 & d_{mpc} \\ 0 & 1 \end{bmatrix} = \begin{bmatrix} 1 & 0 \\ -2/R & 1 \end{bmatrix} \begin{bmatrix} 1 & 2d_{mpc} \\ 0 & 1 \end{bmatrix}. \tag{3.1}$$

The other matrix starting from the flat mirror plane M_f is

$$M_{\mathrm{f}} = \begin{bmatrix} 1 & d_{mpc} \\ 0 & 1 \end{bmatrix} \begin{bmatrix} 1 & 0 \\ -2/R & 1 \end{bmatrix} \begin{bmatrix} 1 & d_{mpc} \\ 0 & 1 \end{bmatrix}. \tag{3.2}$$

For numbering the spots on the MPC mirrors, we use a spot index number i starting from zero to n. i=0 indicates the initial input beam and i=n is the outgoing beam number. So remaining index numbers (i=1 to n-1) correspond to the reflected spots on the mirrors.

We also defined two functions $q_f(i)$ and $q_c(i)$ which return the q-parameter of the i^{th} spot on the flat and curved MPC mirrors respectively. As shown in Figure 3-3, $q_c(0)$ is the q-parameter of the entering beam (q_o) on the input surface, $q_f(1)$ describes the first spot on the flat mirror and finally $q_f(n)$ describes the n^{th} spot on the plane of the flat mirror, which is the outgoing beam through the notch of the flat mirror. Because of the q-preserving property of the MPC, $q_c(0)$ is equal to $q_c(n)$. Using the matrices defined above, we can write the q-parameter of the curved mirror spots as

$$q_c(i) = M_{\mathrm{c}}^i \cdot q_0 \quad , \quad 1 < i < n. \tag{3.3}$$

For flat mirror spots, since our unit cell starts from the plane of the flat mirror, we also need a simple free space transfer matrix for calculating the first beam $q_f(1)$ on the flat mirror. The ray transfer matrix for a free space length of d_{mpc} is given by

$$M_d = \begin{bmatrix} 1 & d_{mpc} \\ 0 & 1 \end{bmatrix}. \tag{3.4}$$

Now the q-parameter of the first spot on the flat mirror has the form

$$q_f(1) = M_d \cdot q_o. \tag{3.5}$$

Therefore, we can write the q-parameters of the other beams on the flat mirror as

$$q_f(i) = M_f^{\mathrm{i-1}} \cdot q_f(1) \quad , \quad 1 < i < n. \tag{3.6}$$

Finally, in view of Equations 3.5 and 3.6, we have

$$q_f(i) = \left(M_f^{i-1} \cdot M_d\right) \cdot q_0 \quad , \quad 1 < i < n. \tag{3.7}$$

Equations 3.3 and 3.7 give us the q-parameters of all the spots on the both MPC mirrors.

3.1.2 Spot Size of the Beams

The q-parameter of a Gaussian beam which involves the spot size and wave front curvature of the beam is defined by [26]

$$\frac{1}{q} = \frac{1}{R} + j\,\frac{-\lambda}{\pi w^2}, \tag{3.8}$$

where R is the radius of curvature of the wavefront, λ is the wavelength of the beam in the medium and w is the spot size. As a result we can write the spot sizes a function of q parameter:

$$w = \sqrt{\frac{-\lambda}{\pi \operatorname{Im}\left(q^{-1}\right)}}. \tag{3.9}$$

Using Equation 3.9, we can directly use the q-parameters calculated by the matrix transfer method to obtain the spot sizes of the beams on each mirror.

3.1.3 Measuring the q-Parameter of the Entering Beam (q_o)

For calculating the spot size of the beams on the MPC mirrors, we first need to know the q-parameter of the entering beam. We can calculate this theoretically from the short cavity analyses, but for exact matching to the experimental conditions it is much more accurate to measure it.

For calculating the q-parameter, we need two factors: the spot size and the wavefront radius of curvature. Considering the fact that the input plane of the MPC is the flat mirror plane of the short cavity, the wavefront radius of curvature of the beam will be infinite at this plane. Therefore according to equation 3.8, the q-parameter must be purely imaginary at this plane and the spot size will be equal to the beam waist radius.

$$\frac{1}{q_o} = -j\frac{\lambda}{\pi w_o^2} \Rightarrow q_o = j\frac{\pi w_o^2}{\lambda}. \tag{3.10}$$

As a result, we only need to measure the radius of the beam waist to calculate q_o.

For measuring the beam waist, before the construction of the MPC cavity, we used a flat output coupler instead of the high reflecting end mirror of the short cavity. Since making a measurement at the exact location of the plane of the mirror was not possible, we measured the spot size at two different distances from the output coupler as shown in Figure 3-5 by using the knife-edge technique. (See Appendix I.)

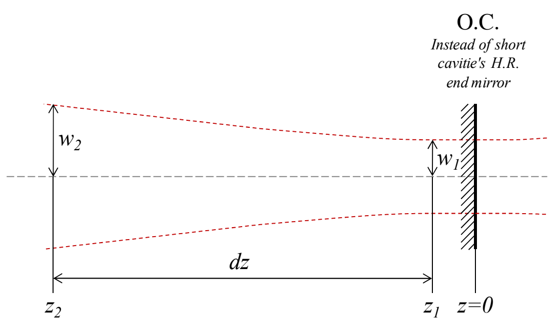

Figure 3-5 - Measuring q-parameter of the input beam

We measured w_1=183μm at about 1.5cm from the mirror's back side (minimum possible distance), w_2=810μm at distance dz = 55cm from the z_1 plane.

Using Equation 3.8, we can express the Gaussian beam spot size as a function of the distance from the beam waist that we label by z. This yields

$$w(z) = w_o\sqrt{1+\left(\frac{\lambda z}{\pi w_o}\right)^2}. \tag{3.11}$$

Numerical solution of Equation 3.11 as a set of two equations with measured values[1] resulted in two sets of solutions for z_1 and w_o.

$$\begin{cases} w(z_1) = w_1 \\ w(z_1 + dz) = w_2 \end{cases} \Rightarrow \begin{cases} z_1 = 23.15mm \\ w_o = 180.2\mu m \end{cases}, \begin{cases} z_1 = -62.28mm \\ w_o = 150.2\mu m \end{cases}$$

As shown in Figure 3-5, z_1 and z_2 are both located on the left side of the beam waist, which we take as the positive direction, so the first set is acceptable. The beam waist w_o is close to w_1 and considering the thickness of the mirror, z_1 is close to our expected value. Using equation 3.10, we find j0.13049 for the numeric value of q_o.

3.1.4 Position of the Spots on the MPC Mirrors

The total number of the spots on each mirror is equal to n, and since the last one goes out through the notch of the mirror, the number of visible spots is n-1. By definition of the q-preserving property, these n spots occur in m half circles or m·π radians. Therefore, the angular advance between spots is m·π /n radians, and if we write this angle as a function of the spot index number i, we have

$$\theta(i) = \frac{\pi m}{n} i \tag{3.12}$$

The beam patterns on the mirrors can, in general, be elliptic due to the initial offset or angle of inclination, but for simplicity we assume ideal circular patterns. In this case, the x and y coordinates of the spots on the MPC mirrors are given by

$$\begin{cases} x_c(i) = \rho_{pat-c} Cos\left(\theta(i)\right) \\ y_c(i) = \rho_{pat-c} Sin\left(\theta(i)\right) \end{cases} \tag{3.13}$$

$$\begin{cases} x_f(i) = \rho_{pat-f} Cos\left(\theta(i)\right) \\ y_f(i) = \rho_{pat-f} Sin\left(\theta(i)\right) \end{cases} \tag{3.14}$$

[1] λ=780nm

Here ρ_{pat-c} and ρ_{pat-f} are the radii of the patterns on the curved and flat mirrors respectively. Figure 3-6 shows the location of the i^{th} spot on the MPC mirrors.

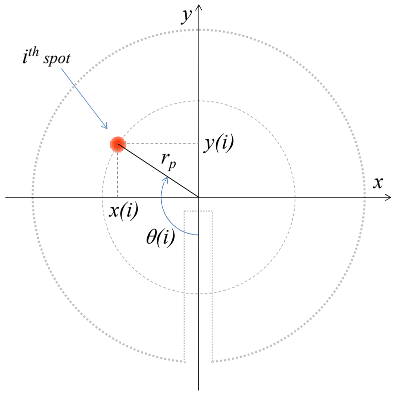

Figure 3-6 - Coordinates of the i^{th} spot on the MPC mirrors

3.1.5 Pattern radii on the MPC mirrors

The radius of the forming pattern on the curved mirror is an adjustable parameter which can be adjusted easily by shifting the MPC mirror's position with respect to the input beam. The radius of the pattern on the flat mirror has a fixed ratio to the radius of the pattern on the curved mirror. The ratio between pattern radii for flat-curved design is as follows [27].

$$\rho_{pat-f} = \rho_{pat-c} Cos\left(\frac{m\pi}{2n}\right). \tag{3.15}$$

According to Equation 3.15, the pattern radius of the flat mirror cannot be larger than the pattern radius of the curved mirror, and for a fixed m value, increasing n causes small pattern radius on the flat mirror.

3.1.6 Calculation of the Spot Sizes

In our standard MPC design we implemented an MPC cavity with m=4, n=11 using R=2m curved mirror. The MPC length for this configuration using Equation 2.2 is

$$d_{mpc} = \frac{R}{2}\left(1 - Cos\left(\frac{m\pi}{n}\right)\right) = 0.5845m$$

Now using Equations 3.3, 3.7, 3.9 and the calculated MPC length and q-parameter of the entering beam, we can calculate the q-parameters and the spot sizes. Table 3.1 shows the simulation results for this configuration.

i	θ(°)	w_c(mm)	w_f(mm)
1	65.45	1.621	0.825
2	130.9	1.339	1.477
3	196.4	0.539	0.436
4	261.8	1.759	1.139
5	327.3	0.961	1.355
6	32.73	0.981	0.151
7	98.18	1.755	1.364
8	163.6	0.518	1.126
9	229.1	1.354	0.453
10	294.5	1.611	1.479
11	0	0.180	0.808

Table 3-1 - Simulation results for m=4, n=11 configuration.

3.2 Visualization of the Simulations

Using the calculated spot size values and coordinates of the spots, we can visualize the final results of the simulations of the mirrors. These visualizations can easily show all the losses and other problems. To this end, we only need to plot their spatial intensities.

3.2.1 Intensity of the spots

The propagating beams on the mirrors are lowest order TEM_{00} Gaussian beams. Spatial intensity of these beams is a Gaussian distribution. Thus for a spot located at (x_o, y_o) with a spot size of w, its spatial intensity function (neglecting astigmatism) will be

$$I(x,y)=\frac{2P}{\pi w^2}e^{-2\frac{\left((x-x_o)^2+(y-y_o)^2\right)}{w^2}}, \tag{3.16}$$

where I(x, y) is the intensity at the x, y coordinates, P_o is the beam power, w is the spot size, and (x_o, y_o) is the location of the spot's center.

3.2.2 Gamma Correction

For best visualization and comparability with the real beam patterns, we also need to do gamma correction for our simulated spots. Gamma correction is helpful in mapping data into a more perceptually uniform domain. In the simplest cases, the gamma factor γ, is defined by the following power-law expression [28]

$$I=v^{\gamma}. \tag{3.17}$$

Here I is the intensity (linear luminance) and v is the pixel level, both normalized to take real values between 0 to 1. In standard computer displays, the value of gamma is 2.2.

For applying the gamma correction to our spot intensities, we must apply equation 3.17 for calculating the pixel levels, namely

$$v=I^{\frac{1}{\gamma}}. \tag{3.18}$$

3.2.3 Visualization Results

Figure 3-7 shows the visualization of the results, and Figure 3-8 shows the actual patterns on the mirrors that were photographed and then scaled for better comparability.

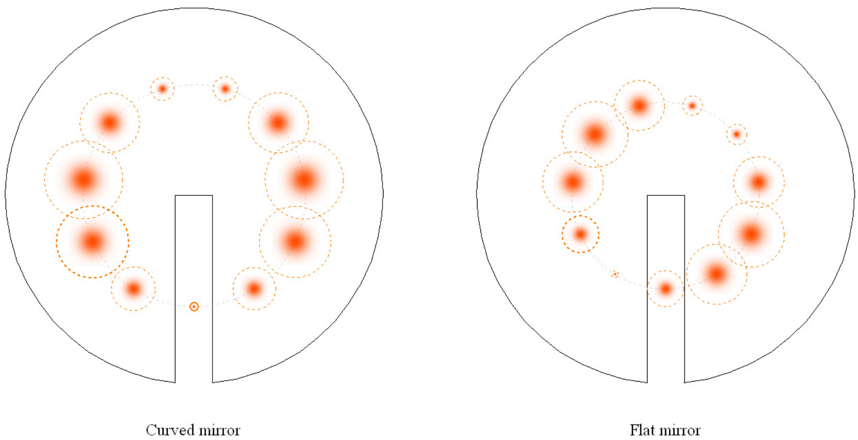

Figure 3-7 - Simulated patterns for MPC mirrors (m=4 and n=11).

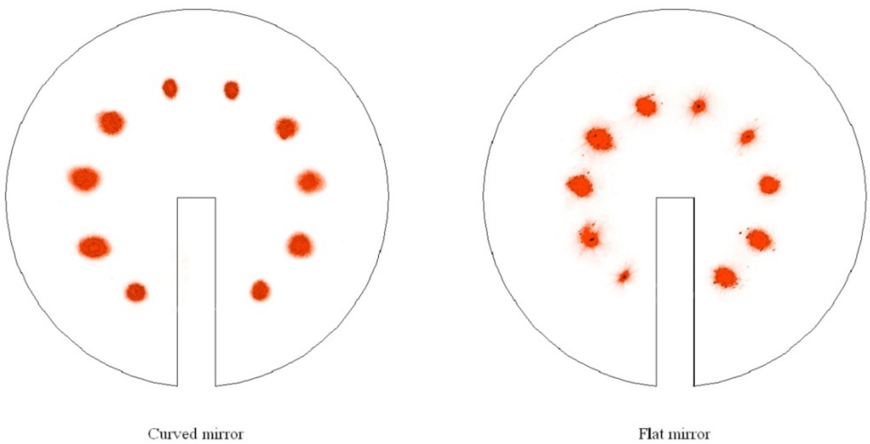

Figure 3-8 - Actual patterns on the MPC mirrors (m=4 and n=11).

As shown in Figure s 3-6 and 3-7 the simulation results are very close to the real spots. The dashed circles around the simulated spots are the 3w radius[1] of the spots which contain almost all of the beam power.

The 3w dashed lines easily show the clipping losses. In this configuration, the clipping losses are close to zero, because the 3w areas for the reflected beams are completely covered by the mirror surfaces, and for the center beams these areas completely pass through the notches. Figure 3-9 shows the spot patterns on the flat MPC mirror of our experimental setup.

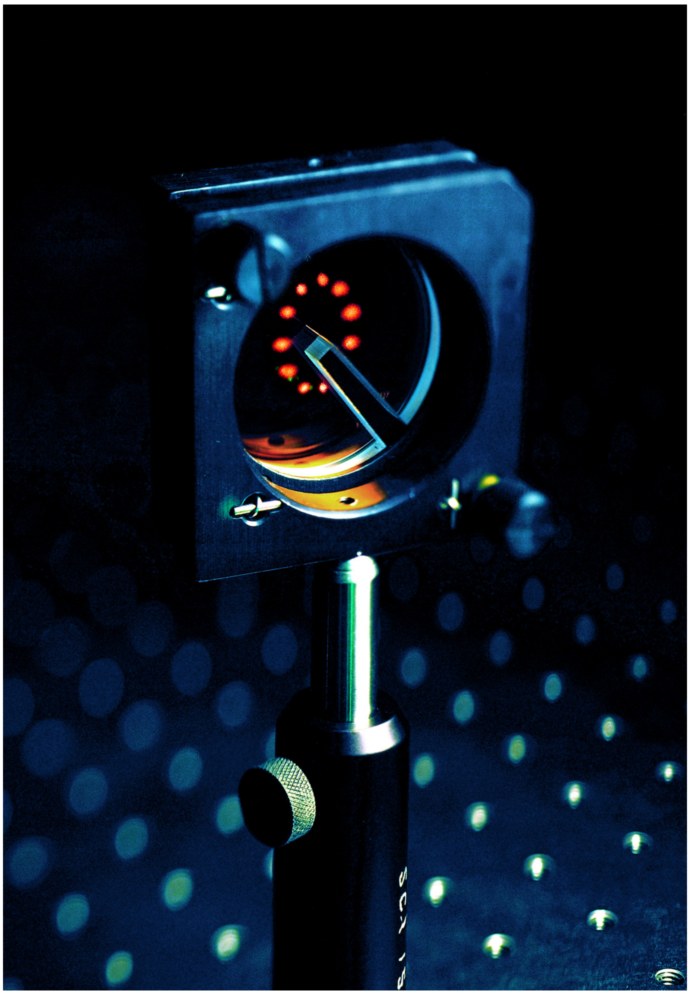

Figure 3-9 - Spot pattern on the flat MPC mirror of our experimental setup.

[1] The thicker dashed circle indicates the first spot on the mirror (i=1).

4 Optical Losses in the MPC

In general, there are two main sources of loss in laser cavities; reflection and clipping losses. Reflection losses depend on the quality of the mirrors and clipping losses are due to the finite surface of the mirrors. In addition to the ordinary surface clipping losses, there can be high losses during the passage of the input and output beams at notches of the MPC mirrors. These losses can be significant when the beam radii are comparable with notch dimensions. In typical MPC designs, the diameter of the input and output beams are assumed to be small enough in relation to the width of notches. In this case, these losses are negligible.

4.1 Reflection losses in the MPC

In MPCs, since the optical beam will be reflected n-1 times on each mirror, there will be 2(n-1) reflections for one pass and 4(n-1) in total. Figure 4-1 shows the MPC structure of our experimental setup. In our MPC design, there is dispersion compensating which introduce negative group velocity dispersion into the cavity. These elements have reflection losses that must be taken into account. Therefore, the round-trip transmission $T_{reflection}$ of the MPC can be expressed as

$$T_{reflection} = R_{mpc}^{4(n-1)} \cdot R_{dispersion}. \tag{4.1}$$

Here, R_{mpc} is the reflection coefficient of the MPC mirrors which is assumed to be identical for both MPC mirrors and $R_{dispersion}$ is the reflection coefficient of the additional dispersion compensating mirrors (GTI mirrors in our setup). We assumed that the reflection coefficient of the compensating end mirror (M_C) is equal to that of the short cavity high reflection mirror, which is replaced by the MPC cell.

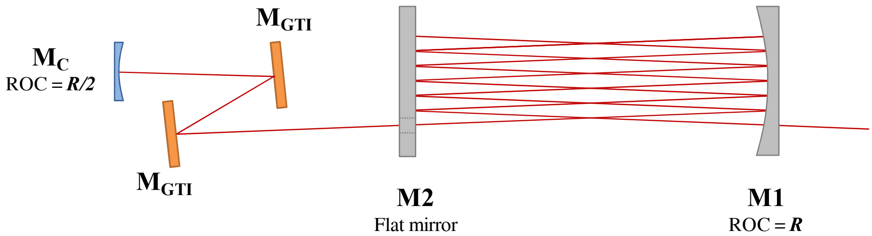

Figure 4-1 - MPC cell and dispersion compansating mirrors

Figure 4-1 shows our experimental MPC setup. We use two GTI mirrors for dispersion compensation. Each of these reflects the beam twice in one complete passage of the beam through the MPC. So,

$$T_{reflection} = R_{mpc}^{4(n-1)} \cdot R_{gti}^{4}, \tag{4.2}$$

where R_{gti} is the reflection coefficient of the GTI mirrors.

4.2 Clipping Losses of the MPC

There are three kinds of clipping losses in the MPC cell: 1) Clipping of the center spots during the passage through the notches, 2) Clipping of the spots adjacent to the notches and 3) Surface clippings of all spots on the MPC mirrors. In order to calculate these losses, first we need an analytic formula that describes the clipping of a Gaussian beam by a straight cut edge.

4.2.1 Clipping Loss of a Gaussian Beam by an Edge

Figure 4-2 shows a lowest order TEM_{00} Gaussian beam clipped by an edge.

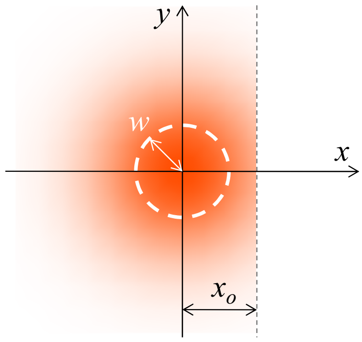

Figure 4-2 - Clipping of a Gaussian beam by an edge

By definition, the intensity distribution of the lowest order Gaussian beam in polar coordinates is given by

$$I(r) = \frac{2P_o}{\pi w^2} e^{-2\frac{r^2}{w^2}}, \tag{4.3}$$

where P_o is the beam power and w is the beam spot size. Changing to Cartesian coordinates, we find the following formula for the transmitted power by the Gaussian beam.

$$P_T = \frac{2P_o}{\pi w^2} \int_{-\infty}^{+\infty} dy \int_{-\infty}^{\Delta x} dx \cdot e^{-2\frac{x^2+y^2}{w^2}}. \tag{4.4}$$

As shown is Figure 4-2, Δx is the distance of the edge from the spot center and w is the spot size. Dividing the transmitted power by the initial beam power results in the transmission expression given by

$$T_{edge} = \frac{1}{2}\left(1 + Erf\left(\frac{\sqrt{2}\Delta x}{w}\right)\right). \tag{4.5}$$

Equation 4.5 is our key equation in calculating all of the clipping losses on the MPC mirrors.

4.2.2 Center Spot Analysis

One of the constraints for choosing the MPC configuration is the size of the center spots that pass through the notches. The center spot for the curved mirror is the input beam and its size depends on the short cavity parameters. However, the center spot for the flat mirror depends on the MPC parameters. Now we can calculate the size of the last spot on the flat mirror for various m and n combinations. Without any loss calculations, we know that for a lossless passage of a Gaussian beam through an aperture, the spot size must be smaller than 1/3 of the aperture radius or 1/6 of its diameter. In our experimental setup, the input beam radius is around 180 μ m and it is small compared to the notch width of 5mm. Now, we can calculate the center spot size for the flat mirror and compare it with the notch width. Figure 4-3 shows the center spot size in millimeters for different (m,n) values and the 1/6 of the notch width as a gray dashed line for comparison.

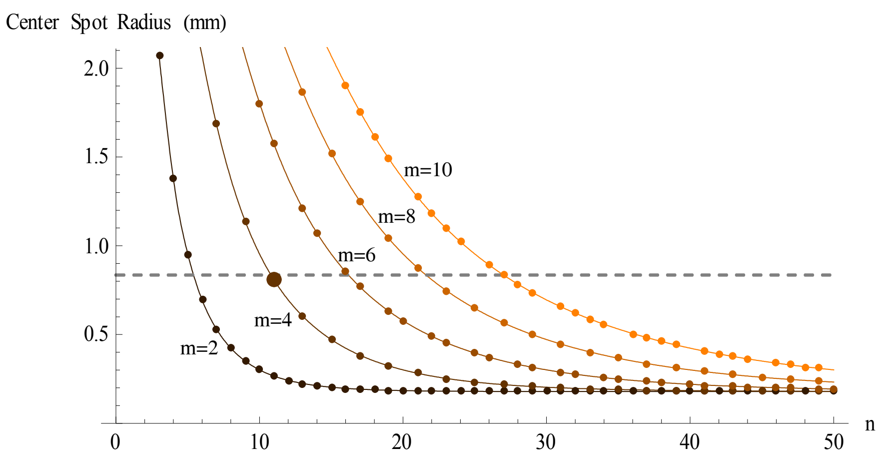

Figure 4-3 - Center spot size on the MPC flat mirror[1]

Considering the center spot constraint, the best and simplest possible configuration according to Figure 4-3 is m=4 and n=11[2] which is shown as a bigger point on the graph.

[1] Circular points are the realizable configurations.
[2] There are also other configurations near this criteria such as m=10, n=27 or m=6, n=16, but due to the large n values these configurations are hard to implement in practice.

4.2.3 Clipping Losses of the Center Spots

As shown is Figure 4-4, the center spots which pass through the notches are clipped from both sides by the notch edges.

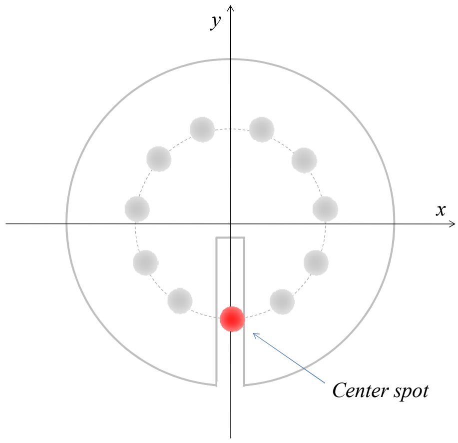

Figure 4-4 - Center spot

The distance of the edge to the spot is equal to half of the notch width;

$$\Delta x = \frac{w_{notch}}{2}. \tag{4.6}$$

Therefore, in view of Equation 4.5 and under the assumption that the notch width for both mirrors is identical, the clipping losses for the center spot on the curved and flat MPC mirrors are given by

$$T_{center-c} = \frac{1}{4}\left(1 + Erf\left(\frac{\sqrt{2}w_{notch}}{2w_c(0)}\right)\right), \tag{4.7}$$

$$T_{center-f} = \frac{1}{4}\left(1 + Erf\left(\frac{\sqrt{2}w_{notch}}{2w_f(n)}\right)\right). \tag{4.8}$$

The center spot size for the curved mirror $w_c(0)$ is the spot size of the entering beam to the MPC or simply w_o and the center spot size for the flat mirror will be $w_f(n)$. w_{notch} is the width of the notches.

The total center spot transmission is obtained by multiplying Equations 4.7 and 4.8 and squaring the result to account for the round trip:

$$T_{center} = \left(\frac{1}{16}\left(1 + Erf\left(\frac{\sqrt{2}w_{notch}}{2w_o}\right)\right)\left(1 + Erf\left(\frac{\sqrt{2}w_{notch}}{2w_f(n)}\right)\right)\right)^2. \tag{4.9}$$

Figure 4-5 shows the total two pass center spot clipping losses for various configurations.

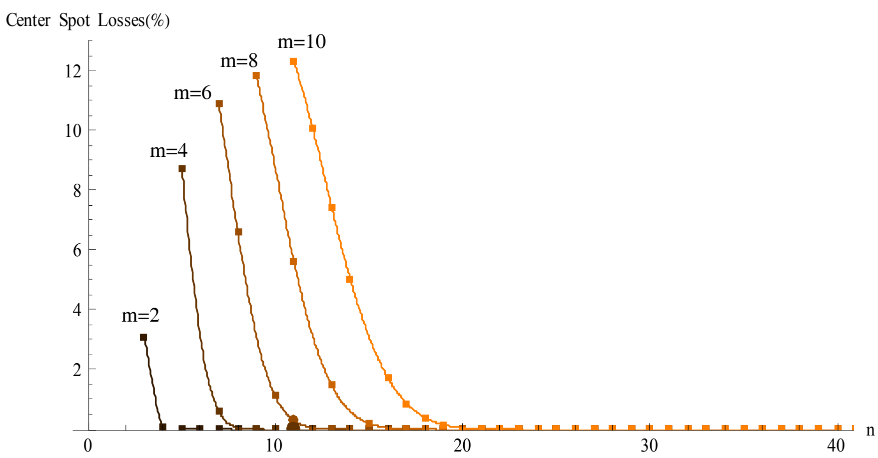

Figure 4-5 - Center spots clipping losses

4.2.4 Clipping Losses of the Adjacent Spots

Figure 4.6 shows the adjacent spots to the notches on both mirrors.

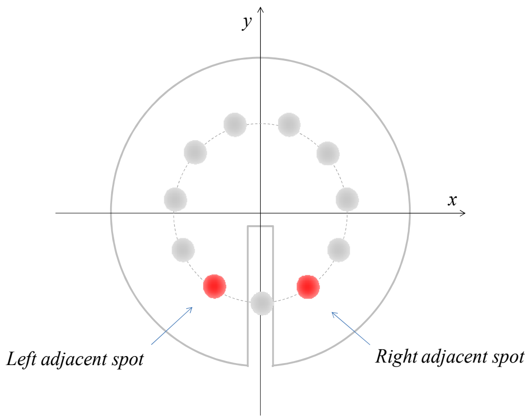

Figure 4-6 - Adjacent spots of the notches

Each of these spots is clipped from one side by the notch edge. For calculating the distance between the notch edge and the spot center, we will need the coordinates of the adjacent spots and we need to calculate their index number.

The index numbers of the adjacent spots on both MPC mirrors are identical. Using simple geometry, the index number for the left and right spots can be expressed as

$$i_L = \frac{2(kn+1)}{m}, k \in \mathbb{Z}, \tag{4.10}$$

$$i_R = \frac{2(k'n-1)}{m}, k' \in \mathbb{Z}. \tag{4.11}$$

However, these results cannot be used directly as a function. For solving this problem, we use an alternative algorithm. We know that for even m values, the n spots are equally spaced on a circular or elliptic pattern. The angular distance between the spots is $2\pi/n$. So for any combination with even m,

$$\theta(i_L) = \frac{2\pi}{n} + 2\pi k, \tag{4.12}$$

$$\theta(i_R) = 2\pi\left(1-\frac{1}{n}\right)+2\pi k'. \tag{4.13}$$

Here k and k' are integers. So we can use loops, running for all m and n values in the range and check the following condition for each combination to find the i_L and i_R. For eliminating the integer multiples of the full circular roundtrips from the spot angle, we use Integer-Part functions.

$$If\ \theta(i)-\left(2\pi\cdot Int\left[\frac{\theta(i)}{2\pi}\right]\right)=\frac{2\pi}{n}\Rightarrow i_L=i, \tag{4.14}$$

$$If\ \theta(i)-\left(2\pi\cdot Int\left[\frac{\theta(i)}{2\pi}\right]\right)=2\pi\left(\frac{n-1}{n}\right)\Rightarrow i_R=i. \tag{4.15}$$

Then, for using the result of the loops, we define m × n matrices to store the results. The loop that we use checks the conditions given by 4.14 and 4.15 for all m and n values in the range, and if these conditions are fulfilled, it stores the value of ***i*** to the (m, n) component of the matrix.

$$L_{m,n}=i_L(m,n), \tag{4.16}$$

$$R_{m,n}=i_R(m,n). \tag{4.17}$$

An interesting point about the index numbers of the adjacent spots is that the sum of left and right adjacent spots are equal to n[1]. Therefore, we need only calculate and store one of them.

Another interesting side result of this conditional loop is for checking the realizable m and n combinations. For available combinations, the left adjacent spot number will be found through the loop running for i=1 to n. However, for combinations that cannot be realized, there will be no ***i*** value satisfying the above condition. We have used this algorithm for checking the availability of the configurations. We defined a Boolean valued matrix whose (m, n) component shows the availability of the m and n combination.

---

[1] It can be easily shows if we calculate the left and write adjacent spot index numbers for realiazble combinations and then add them.

From our previous calculations, the spot size and coordinates of all of the spots are available. Considering the symmetry, the distance of the notch edge from the left and right spots is identical and is equal

$$\Delta x_c = \left|x_c(i_L)\right| - \frac{w_{notch}}{2} = \left|x_c(i_R)\right| - \frac{w_{notch}}{2}, \tag{4.18}$$

$$\Delta x_f = \left|x_f(i_L)\right| - \frac{w_{notch}}{2} = \left|x_f(i_R)\right| - \frac{w_{notch}}{2}. \tag{4.19}$$

Now using the calculated spot sizes with calculated distances, the clipping losses of the adjacent spots for both mirrors will be

$$T_{adjacent-c} = \frac{1}{4}\left(1 + Erf\left(\frac{\sqrt{2}x_c}{w_c(i_L)}\right)\right)\left(1 + Erf\left(\frac{\sqrt{2}x_c}{w_c(i_R)}\right)\right) \tag{4.20}$$

$$T_{adjacent-f} = \frac{1}{4}\left(1 + Erf\left(\frac{\sqrt{2}x_f}{w_f(i_L)}\right)\right)\left(1 + Erf\left(\frac{\sqrt{2}x_f}{w_f(i_R)}\right)\right). \tag{4.21}$$

Multiplying Equations 4.20 and 4.21, we find the following expression for the total adjacent spots transmission for two pass complete round trip.

$$T_{adjacent} = \left(\frac{1}{16}\left(1 + Erf\left(\frac{\sqrt{2}x_c}{w_c(i_L)}\right)\right)\left(1 + Erf\left(\frac{\sqrt{2}x_c}{w_c(i_R)}\right)\right)\left(1 + Erf\left(\frac{\sqrt{2}x_f}{w_f(i_L)}\right)\right)\left(1 + Erf\left(\frac{\sqrt{2}x_f}{w_f(i_R)}\right)\right)\right)^2. \tag{4.22}$$

Figure 4-7 shows the total adjacent spot clipping losses for various configurations in our experimental setup.

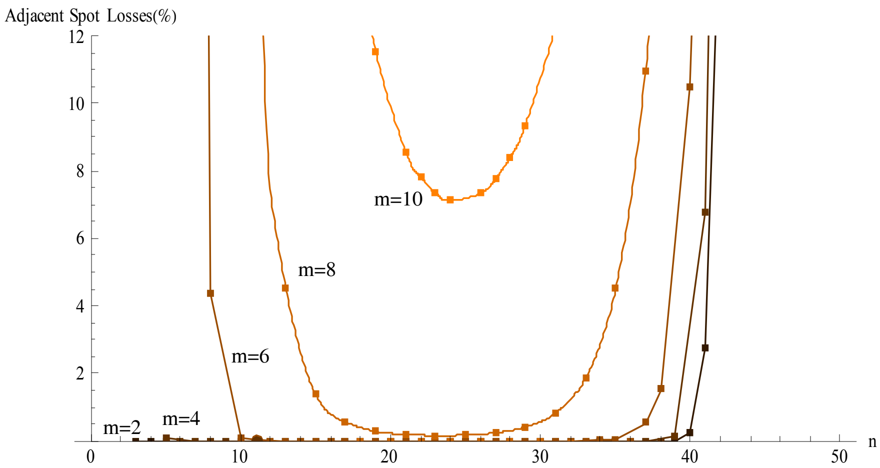

Figure 4-7 - Adjacent spots clipping losses

The radius of the pattern on the curved mirror in our experimental setup was adjusted to be around 16mm. Analyzing spot size and other parameters for this graph has an important consequence. The high losses for small n values are due to the large spot sizes, but for large n values the loss comes from the decreasing angular space between the spots and also the reduction of the pattern radius on the flat mirror. Since the ratio of the radius on the flat mirror to the pattern radius on the curved mirror is constant for each combination, we must adjust the pattern radius on the curved mirror to take largest possible value. Although increasing the pattern radius on curved mirror will increase the surface losses, we can find an optimum radius. We discuss this issue in Chapter 6.

4.2.5 Surface Clipping Losses on MPC mirrors

Due to the finite surface of the MPC mirrors, there are clipping losses for each spot. In general, the MPC mirrors seem to be large enough to neglect these losses. However, in some cases the spot sizes can become very large and introduce large amount of losses. For example, Figure 4-8 shows the simulation result for m=8 and n=11 configuration.

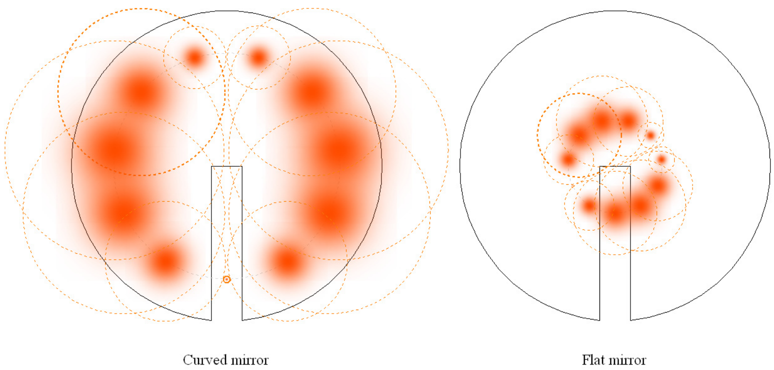

Figure 4-8 - Simulation result showing the spot pattern for m=8, n=11 configuration.

As seen in Fig. 4-8, the spots become very large and there are very high losses on the curved MPC mirror. For calculating these clipping losses, we need to calculate the amount of transmission. This is similar to our treatment of the losses due to the knife-edge clipping. Unfortunately, the resulting integrals become too complicated to allow for an explicit evaluation. For solving this problem, we approximate the circular shape of the MPC mirrors with an n-sided polygon. See Figure 4-9.

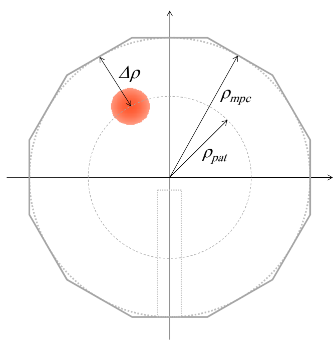

Figure 4-9 - Polygon approximation for surface loss calculations

In this case we can use the knife-edge transmission formula for calculating the loss of each spot. As a result of this approximation, the distance of each spot to the edge of the mirror is equal to the difference between radius of the mirror and the radius of the pattern. We use Δρ instead of Δx for this value.

$$\Delta\rho_c = \rho_{mpc} - \rho_{pat-c}, \tag{4.23}$$

$$\Delta\rho_f = \rho_{mpc} - \rho_{pat-f}. \tag{4.24}$$

Then,

$$T_{surface-c} = \prod_{i=1}^{n-1} \frac{1}{2}\left(1 + Erf\left(\frac{\sqrt{2}(\Delta\rho_c)}{w_c(i)}\right)\right), \tag{4.25}$$

$$T_{surface-f} = \prod_{i=1}^{n-1} \frac{1}{2}\left(1 + Erf\left(\frac{\sqrt{2}(\Delta\rho_f)}{w_f(i)}\right)\right). \tag{4.26}$$

Therefore, the total surface transmission for both mirrors for a complete round trip is

$$T_{surface} = \left(\prod_{i=1}^{n-1} \frac{1}{2}\left(1 + Erf\left(\frac{\sqrt{2}(\Delta\rho_c)}{w_c(i)}\right)\right) \cdot \prod_{i=1}^{n-1} \frac{1}{2}\left(1 + Erf\left(\frac{\sqrt{2}(\Delta\rho_f)}{w_f(i)}\right)\right)\right)^2. \tag{4.27}$$

Figure 4-10 shows the two pass total surface clipping losses for various MPC configurations.

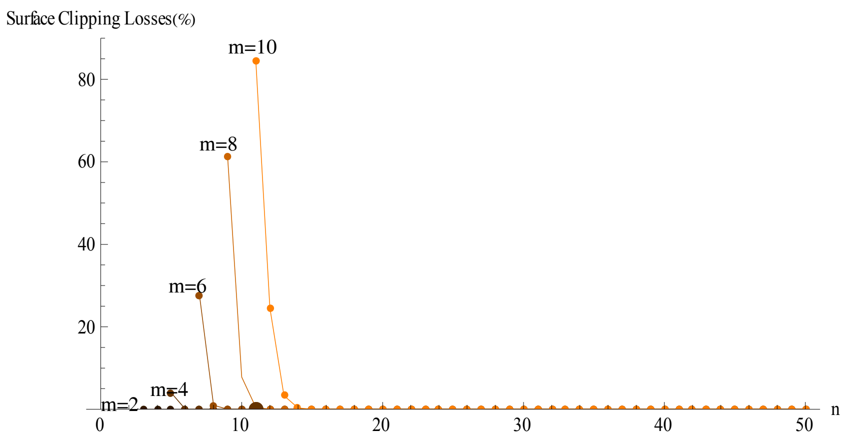

Figure 4-10 - Surface clipping losses for different m and n combinations

In this case, similar to the adjacent spot losses, the radius of the spot pattern is important.

4.2.6 Total MPC Clipping Losses

Total clipping transmission of the MPC is equal to the product of all clipping transmissions;

$$T_{clipping} = T_{center} \cdot T_{adjacent} \cdot T_{surface}. \tag{4.28}$$

Figure 4-11 shows the overall clipping losses for the various MPC configurations except for the reflection losses.

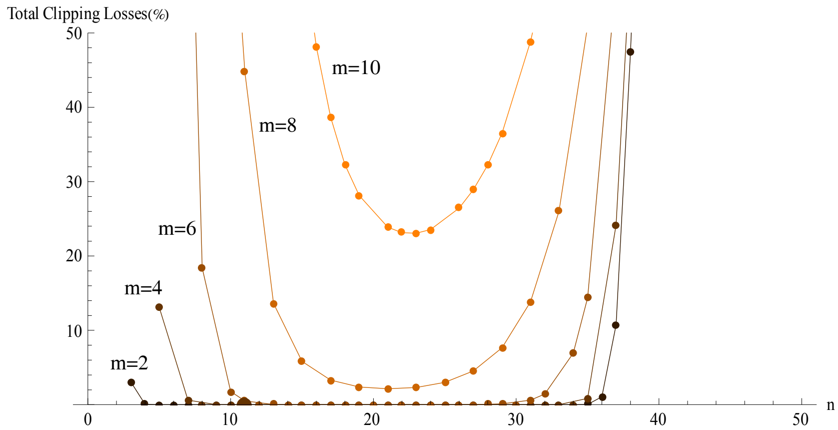

Figure 4-11 - Total clipping losses for different m and n combinations

Table 4-1 shows the total clipping loss values for our experimental setup (m=4, n=11). As expected before, the clipping losses are extremely low.

Center spots losses	1.273×10^{-9}
Adjacent spots losses	1.805×10^{-12}
Surface losses	*0*
Total Clipping losses	$\boldsymbol{1.276\times10^{-9}}$

Table 4-1 - Clipping loss values for m=4 and n=11 configuraion.

5 Laser Power and Energy Analysis

To apply the clipping loss analysis for our laser system, we need some experimental parameters such as mirror reflection coefficients, laser efficiency, etc. We measured these parameters from our standard configuration (m=4, n=11). Figure 5-1 shows the schematics of our experimental setup.

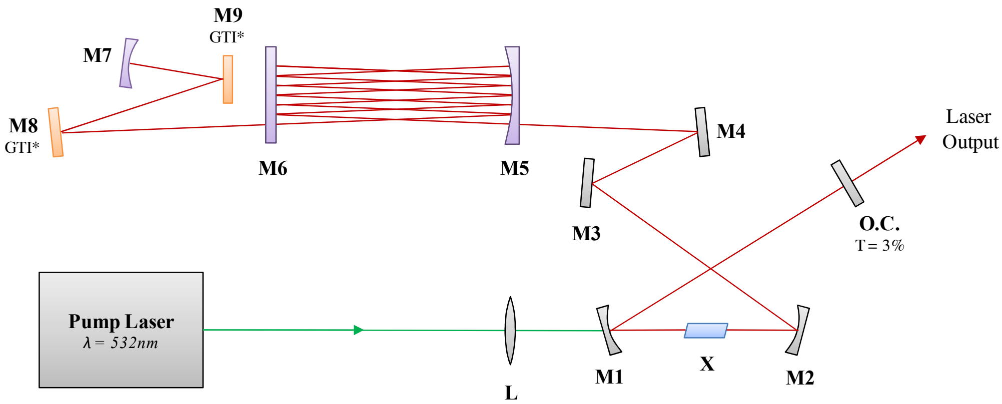

Figure 5-1 - MPC Ti:Sapphirelaser setup

In this setup, we used a focusing lens (L) with 50mm focal length and cavity mirrors (M1 and M2) with radius of curvature (ROC) of 50mm. The crystal is Brewster cut with fractional power absorption of 74% at the pump wavelength of 532nm.

5.1 Dispersion Compensation

For dispersion compensation of the short cavity, we used mirrors with negative group velocity dispersion (GVD) values (M1, M2, M3 and M4). Total negative GVD of the short cavity mirrors was about -410fs^2. In addition to short cavity mirrors, we used two GTI mirrors (M8 and M9) for the extended cavity, each introducing a negative dispersion of -500 + 50 fs^2 per reflection. In our standard configuration (m=4, n=11), the total cavity length was about 14.3m. Assuming +20fs^2/m dispersion for the air and +200fs^2 for the crystal, we found an overall positive dispersion of about +486fs^2. For KLM operation, the total dispersion of the system must be negative. We aimed at a value of around -1000fs^2. Using the GTI mirrors that reflect the beam twice, we achieved an overall GVD of about -1925fs^2 for the standard MPC configuration.[1]

5.1.1 Determination of the System Parameters

To determine our system parameters, first we measured the power efficiency graphs of our experimental system for both the short and extended cavity with standard MPC configurations (m=4 and n=11) as shown in Figure 5-1.

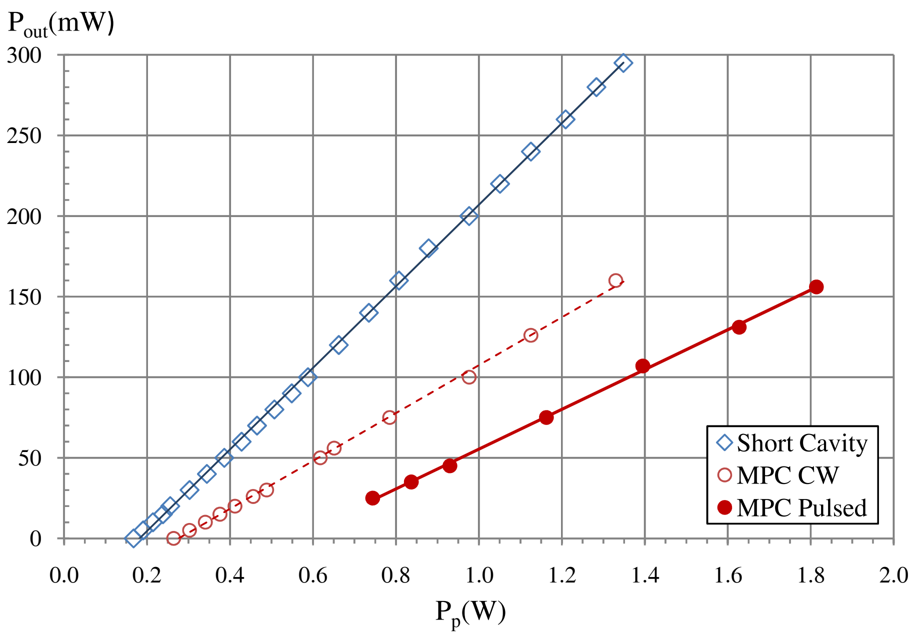

Figure 5-1 - CW power efficiency for short and extended cavity

The pump power (P_p) in Fig. 5-1 is the incident pump power on the crystal. It is determined after accounting for the transmission losses of the focusing lens (L) and M1. We measured the transmission of these elements as 0.93. Based on the measured values in Figure 5-1, we calculated the slope efficiency of the linear best fit line as shown in Table 5-1.

[1] For our optimum configuration (m=6 and n=11) the total cavity length will be increased to 26.6m. The total GVD for the system using GTI mirrors will be around -1650 fs^2, which is sufficient for KLM operation.

	Threshold Power (mW)	*Slope Efficiency*
Short Cavity (CW)	*167.4*	*0.254*
Extended Cavity (Pulsed)	*540.9*	*0.123*

Table 5-1 – Measured lasing threshold power and slope efficieny for the short and extended cavities

Theoretically, the slope of the power efficiency graph or simply, the slope efficiency for low loss values can be expressed as

$$\eta = \frac{\lambda_P}{\lambda_L}\left(\frac{T_{oc}}{L + T_{oc}}\right)\eta_a. \tag{5.1}$$

Here, λ_P and λ_L are the pump and lasing wavelengths and η_a is the fractional power absorption all of which have constant values (λ_P = 532nm, λ_L = 780nm, η_a = 0.74). T_{oc} is the output coupler transmission (T_{oc}=3% in our experimental setup) and L is the total cavity loss. Equation (5.1) works well for low loss values, but for our calculations where high loss values are possible, we must use transmission instead of the loss. This leads to the following modification of Equation (5.1).

$$\eta = \frac{\lambda_P}{\lambda_L}\left(\frac{T_{oc}}{1-\left(T\,(1-T_{oc})\right)}\right)\eta_a. \tag{5.2}$$

Using Equation 4.2 and the measured data of graph 5-1, we can calculate the total transmission. To take into account the short and extended cavity losses, we assumed the total loss to be given by

$$L = L_o + L_{mpc}. \tag{5.3}$$

Here L_o stands for the short cavity losses and L_{mpc} for the additional extended cavity losses. The corresponding transmission takes the form

$$T = T_o \cdot T_{mpc}. \tag{5.4}$$

Similarly, T, T_o and T_{mpc} are total cavity, short cavity, and extended cavity transmissions respectively. We substituted the measured values of the slope efficiency for both the short and extended cavity cases in Equations 5.2 and 5.4 and solved these equations for T_o and T_{mpc}. For short cavity case, the cavity transmission is T_o. Therefore,

$$\eta_{short} = \frac{\lambda_P}{\lambda_L}\left(\frac{T_{oc}}{1-T_o(1-T_{oc})}\right)\eta_a. \tag{5.5}$$

Using our measured data in this equation and solving for T_o, we found $T_o = 0.9692$ ($L_o \approx 3\%$).

As discussed before, the total MPC loss consists of the reflection loss of the dispersion compensating GTI mirrors (M8 and M9) and the reflection loss of the MPC mirror. In our setup, the optical beam reflects four times on the GTI mirrors in one roundtrip. Therefore,

$$T_{mpc} = R_{mpc}^{4(n-1)} \cdot R_{gti}^4. \tag{5.6}$$

Using Equations 5.2, 5.4 and 5.6, we find the following expression for the slope efficiency of the extended cavity.

$$\eta_{klm} = \frac{\lambda_P}{\lambda_L}\left(\frac{T_{oc}}{1-\left(T_o \cdot R_{mpc}^{4(n-1)} \cdot R_{gti}^4\right)(1-T_{oc})}\right)\eta_a. \tag{5.7}$$

According to the technical specifications of our GTI mirrors, their reflection coefficient has the value 99.9%. Substituting the calculated value of T_0 in Equation 5.7 and solving for the reflection coefficient of the MPC mirror, we found $R_{mpc} = 0.998469$.

Now, using the calculated short cavity transmission and reflection coefficient of the MPC mirrors, we can plot the overall system losses for various m and n combinations. Figure 5-2 shows the overall loss of the system including the reflection losses. As shown in the graph, the linear increase in the loss amount is due to the increase in the number of reflections on the MPC mirrors.

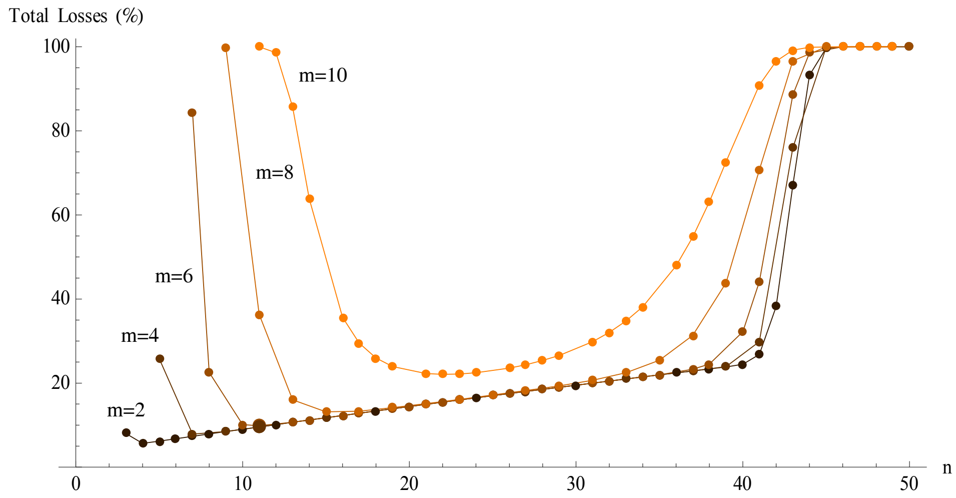

Figure 5-2 - Total losses of the system for different m and n combinations

5.2 Output Power

The average output power of a laser system is equal to,

$$P_{out} = \eta(P_p - P_{th}) \; for \;\; P_p > P_{th}, \tag{5.8}$$

where P_p is the incident pump power on the gain medium, P_{th} is the lasing threshold pump power, and η is slope efficiency. The incident pump power is related to the input pump power with a fixed transmission loss in the focusing lens (L) and the curved mirror (M1). Therefore,

$$P_p = T_{in} \cdot P_{in}, \tag{5.9}$$

where P_{in} is the input pump power that is measured just before the focusing lens and T_{in} is the transmission of optical elements before the crystal. We measured T_{in} to be about 0.93.

The threshold pump power is equal to

$$P_{th} = A(L + T_{oc}), \tag{5.10}$$

where A is a coefficient depending on the operational point of the laser. Replacing the loss with the corresponding transmission value, we find the following modification of Equation 5.10.

$$P_{th} = A\left(1-(T_o T_{mpc})+T_{oc}\right). \tag{5.11}$$

Now using our efficiency graph data, we can calculate the value of A for the KLM operating point. As shown in Figure 5-1, the slope efficiency for extended cavity is approximately the same for the CW and pulsed operation modes. However, the threshold powers are different. The difference comes from the changes in operational point of the system in the CW and pulsed modes. As KLM operation is not possible in low pump powers near lasing threshold, we calculated the threshold power from the linear trend line equation of the output power in KLM operation modes. The result was 540.9mW.

Now, using the value of the threshold power for the KLM operation in Equation 5.11, we calculated the A coefficient as 4.30066.

According to Equations 4.8, 4.9 and 4.10, the output power is given by

$$P_{out} = \eta_{klm}\left(T_{in}\cdot P_{in} - A\left(1-(T_o T_{mpc})+T_{oc}\right)\right), \tag{5.12}$$

or

$$P_{out} = \frac{\lambda_P}{\lambda_L}\left(\frac{T_{oc}\left(T_{in}\cdot P_{in} - A\left(1-(T_o T_{mpc})+T_{oc}\right)\right)}{1-\left(T_o\cdot R_{mpc}^{4(n-1)}\cdot R_{gti}^{4}\right)(1-T_{oc})}\right)\eta_a. \tag{5.13}$$

Now, we can plot Equation 4.12 for various m and n configurations, as shown in Figure 5-3. Here, we have taken the value of the input pump power to be 2.00W.

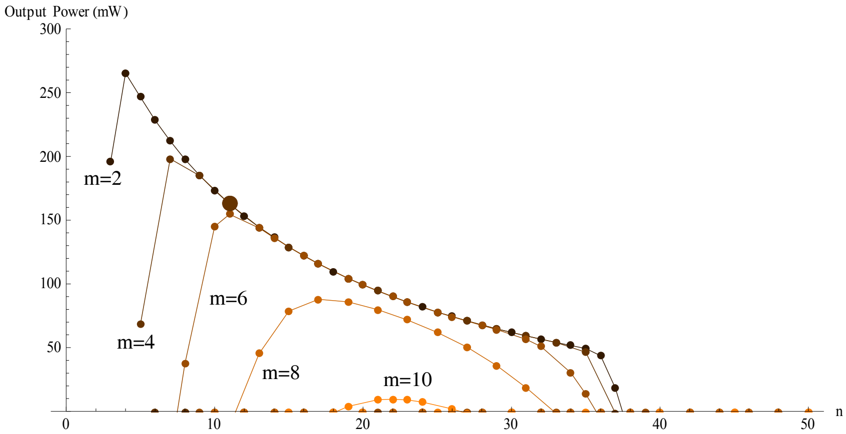

Figure 5-3 - Average output power for various values of m and n

As expected from total loss graphs, the output power decreases after reaching a peak. According to this graph, the m=2 and n=4 configuration gives the highest output power.

Experimentally we measured the output power in KLM operation to be about 107mW with 1.50W of input pump power. The theoretical value calculated using Equation 5.13 is 106.9mW.

5.3 Pulse Energy

For large n and m values, the cavity length becomes longer and pulse repetition rate decreases. Decreasing repetition rate causes the pulse energy to increase. Thus, the pulse energy is proportional to the cavity length. Figure 5-4 shows the cavity length for various configurations.

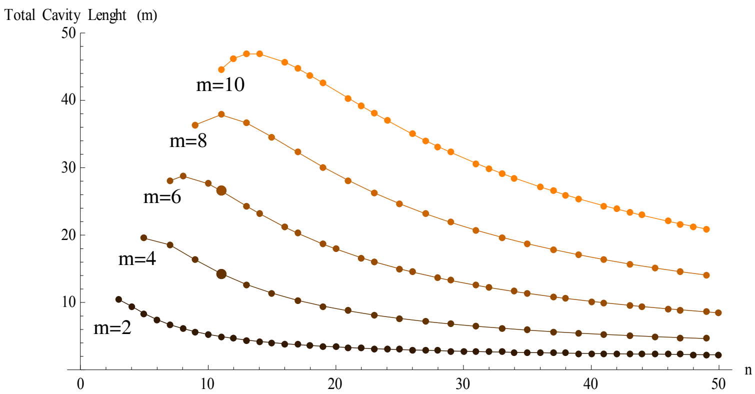

Figure 5-4 - Total cavity lengh for various configurations

Decreasing the repetition rate scales up the pulse energy. Therefore, the pulse energy is proportional to the total cavity length as discussed before.

The repetition rate for the extended cavity is

$$f_{rep} = \frac{c}{2d}, \tag{5.14}$$

where c is the speed of light and d is the cavity length. For our system the cavity length consists of the short and extended parts. Hence,

$$d = d_o + n \cdot d_{mpc}. \tag{5.15}$$

The q-preserving MPC length is given by [29],

$$d_{mpc} = \frac{2}{R}\left(1 - Cos\left(\frac{m\pi}{n}\right)\right). \tag{5.16}$$

Equations 5.14, 5.15 and 5.16 give

$$f_{rep} = \frac{c}{2\left(d_o + \frac{2}{R}\left(1 - Cos\left(\frac{m\pi}{n}\right)\right)\right)}. \tag{5.17}$$

Energy per pulse or the pulse energy has the form

$$W_p = \frac{P_{out}}{f_{rep}}. \tag{5.18}$$

Using the results for the output power and repetition rate, we have

$$W_p = \frac{2\lambda_p \cdot T_{oc} \cdot \eta_a \left(P_p - A\left(1 - (T_o T_{mpc}) + T_{oc}\right)\right)\left(d_o + \frac{2}{R}\left(1 - Cos\left(\frac{m\pi}{n}\right)\right)\right)}{\lambda_L c\left(1 - \left(T_o \cdot R_{mpc}^{4(n-1)} \cdot R_{gti}^{4}\right)(1 - T_{oc})\right)}. \tag{5.19}$$

Figure 5-5 shows the pulse energy for various configurations.

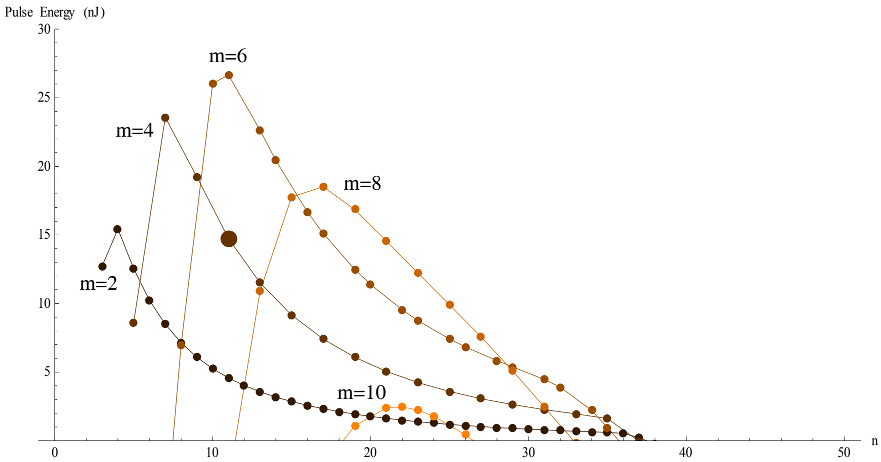

Figure 5-5 - Pulse energy for various configurations

According to Figure 5-5, we expect to achieve the maximum pulse energy in the m=6 and n=11 configuration. As a result of this modeling, the pulse energy improvement relative to our standard design is as large as 85%.

6 Optimum Configuration

Simulation results for the experimentally measured parameters show that m=6 and n=11 is the optimum configuration for our experimental Ti: Sapphire setup. Theoretically, we expect the pulse energy to exceed by a factor of about 81% with respect to the pulse energy of the initial configuration.

Another tunable parameter in the implementation of the optimum design is the pattern radius on the curved mirror of the MPC. Using the clipping loss simulations, we found the optimum value for this radius that led to minimum clipping losses.

6.1 Optimum Pattern Radius

The pattern radius on the curved mirror of the MPC is an adjustable parameter. As the pattern radius becomes larger, the clipping losses for adjacent spots decrease. Since the pattern radius on the flat mirror is smaller than the curved mirror's pattern radius, this type of loss is higher in the flat mirror. On the other hand, the larger pattern increases the surface losses. For finding an optimum value, we can plot the losses as functions of the pattern radius on the curved mirror.

Except for the center spot losses, which do not depend on the pattern radius, the adjacent spot losses and surface losses are highly sensitive to this factor. Figure 6-1 shows the adjacent spot and surface clipping losses as functions of the pattern radius on the MPC curved mirror for the optimum configuration (m=6, n=11).

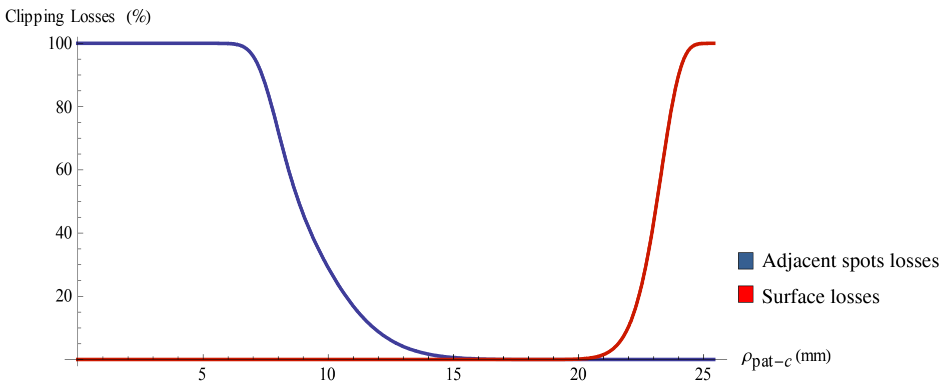

Figure 6-1 - MPC clipping losses as a function of pattern radius

We can also plot the output average power as a function of the pattern radius and take its maximum point as the optimum radius. Figure 6-2 shows the output power for our initial configuration and the optimum configuration. For our initial configuration, there is a wide range of radius values which give the maximum output power. However, in the optimum design, the output power remains close to the maximum value over a much narrower range of radius values as can be seen from Fig. 6.2. This shows that the optimum configuration is highly sensitive to the pattern radius.

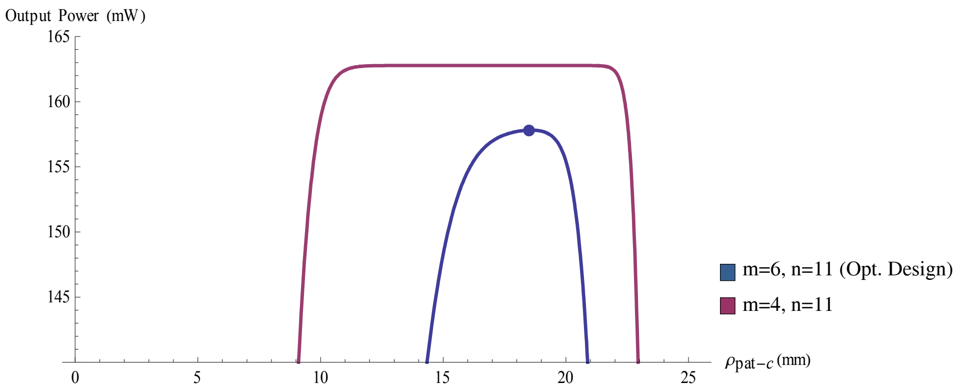

Figure 6-2 - Output power as a function of pattern radius for the initial and optimum MPC configurations

According to this graph, for our optimum configuration with m=6 and n=11, the optimum value for the pattern radius is about 18.5mm.

6.2 Experimental Results

After the construction of the optimum configuration, the experimental results showed slightly higher output power and pulse energy in comparison with our theoretical prediction. According to our calculations, the maximum output power for the optimum configuration is about 175mW in pulsed operation. In the experiments, we measured the output power around 190mW. The experimental results were 8.7% higher than the theoretically expected values.

Table 6-1 shows a summary of all of the experimental results for the KLM operation of the short cavity, initial MPC configuration and the optimum configuration.

	Short Cavity	*Initial Configuration (m=4, n=11)*		*Optimum Configuration (m=6, n=11)*	
		Calculated	*Measured*	*Calculated*	*Measured*
MPC Length (m)	-	0.58		1.1423	
Total Cavity Length (m)	0.72	14.30		26.57	
Repetition Rate (MHz)	208	11.03	~10.9[1]	5.7980	5.8037
Input Pump Power (W)	2	-	1.95	-	2.00
Ave. Output Power (mW)	460.1[2]	157.04	156	174.702	190
Pulse Energy (nJ)	2.21	14.23	14.14[3]	30.13	32.74
Pulsewidth (fs)	N.A.	-	112	-	76.24
Spectral Bandwidth (nm)	N.A.	-	7	-	8.06
Center Wavelenght (nm)	N.A.	-	779.24	-	785.81
Time-Bandwidth product	N.A.	-	0.37	-	0.30
Stability	N.A.	-	>1 hours	-	>1 hours

Table 6-1- Theoretical and experimental results for the initial and optimum configurations.

[1] The pulse energy calculated based on the teoritic value of the repetition rate.
[2] This value is calculated based on the trendline equation.
[3] This pulse energy value is measured with 1.95W of pump power.

For a better comparison, we give in Figure 6-4 the pulse energy for the short cavity, standard configuration, and the optimum configuration.[1]

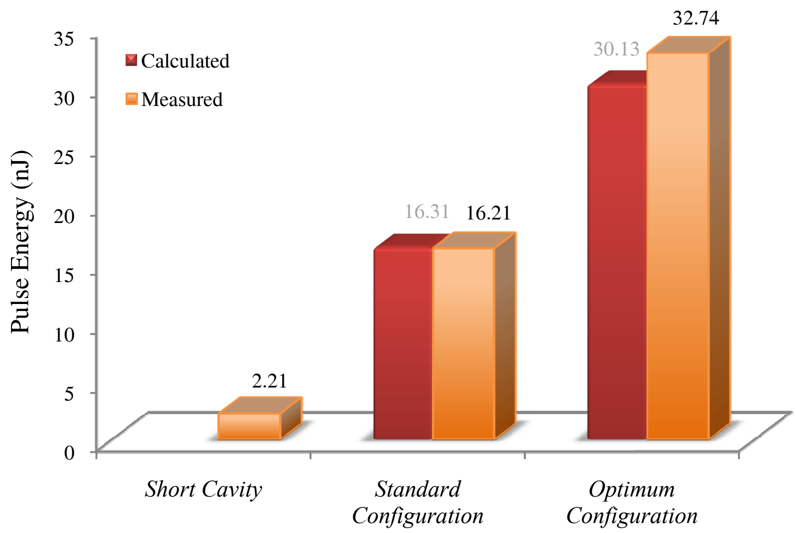

Figure 6-3 - Pulse energy comparison for different configurations.

As a result of our optimization, the achieved pulsed energy was increased by a factor of 101% with respect to the initial configuration.

[1] Because the measured values for the standard design were obtained for a 1.95W input pump power, we recalculated the output power and pulse energies for the 2W input pump power. We also adapted the measured values for the 2W input pump power using the same error relation to the theoretical value.

6.2.1 Horizontally Aligned Notches and Elliptic Spot Shapes

A possible justification for obtaining higher experimental values is the following small change we made in the setup. For an easily adjustable spot pattern radius, we rotated the MPC mirrors and aligned the notches horizontally. In this case, just by shifting the MPC curved mirror, one can adjust the pattern radius easily and accurately. If we look at the spots on the MPC mirrors, we can see that the spots have an elliptic shape. Figure 6-3 shows one of the spots on the flat mirror.

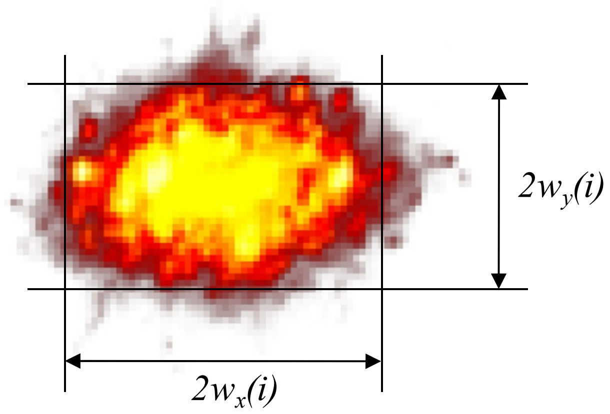

Figure 6-4 - Elliptic shape of the beams on the MPC mirrors

According to the photographs of the spots, the ratio between the spot size in x and y directions is roughly 1.50. This means that, for this spot that corresponds to the passage of the beam through a horizontal notch, the spot size in the vertical (y) direction will be 1.50 times smaller than the one in the horizontal (x) direction. Therefore, the clipping loss for this spot is less than the one corresponding to the passage through a vertical notch. This appears to be a plausible explanation for why the experimental results are somewhat better than the theoretical predictions.

6.3 Pulse Train and Repetition Rate

Figure 6-5 shows the pulse train for the optimum configuration. The pulse train shows a stable single pulsed KLM operation of the system. We measured the repetition rate as 5.8037MHz.

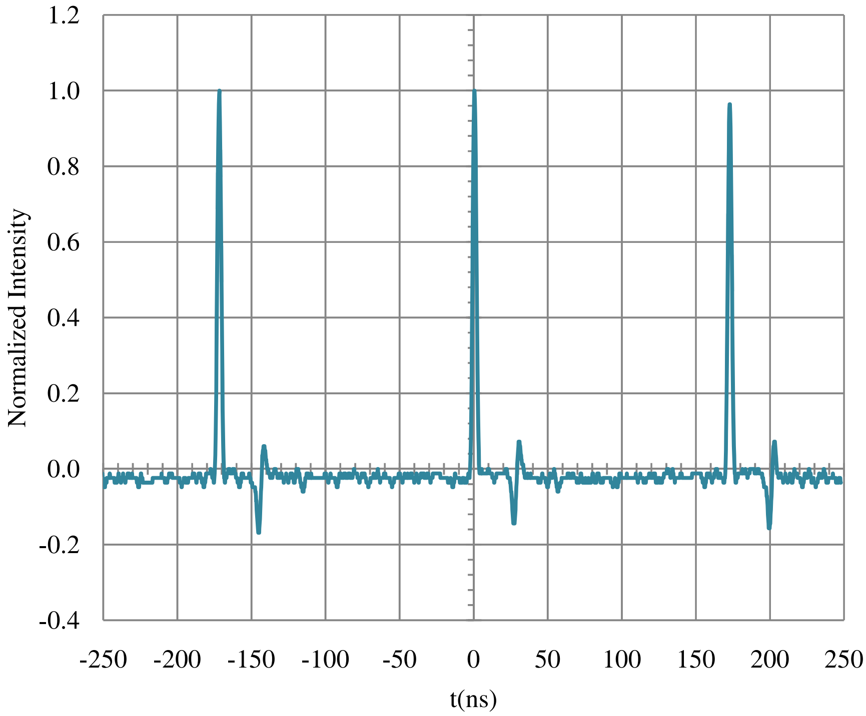

Figure 6-5 - Pulse train of the optimum configuration

6.4 Spectral Bandwidth Results

Figure 6-6 shows the spectral bandwidth of the KLM operation in both the standard and optimum configurations. We measured the spectral bandwidth (FWHM) of around 7.0nm in the standard configuration and 8.1nm in the optimum configuration. There was also a +6.6nm shift in the center wavelength for the optimum configuration. Since the total cavity length changed in the optimum configuration, the overall cavity dispersion was also changed. This change together with the non-linear dispersion/wavelength relation of the GTI mirrors caused a shift in the center frequency of the KLM operation.

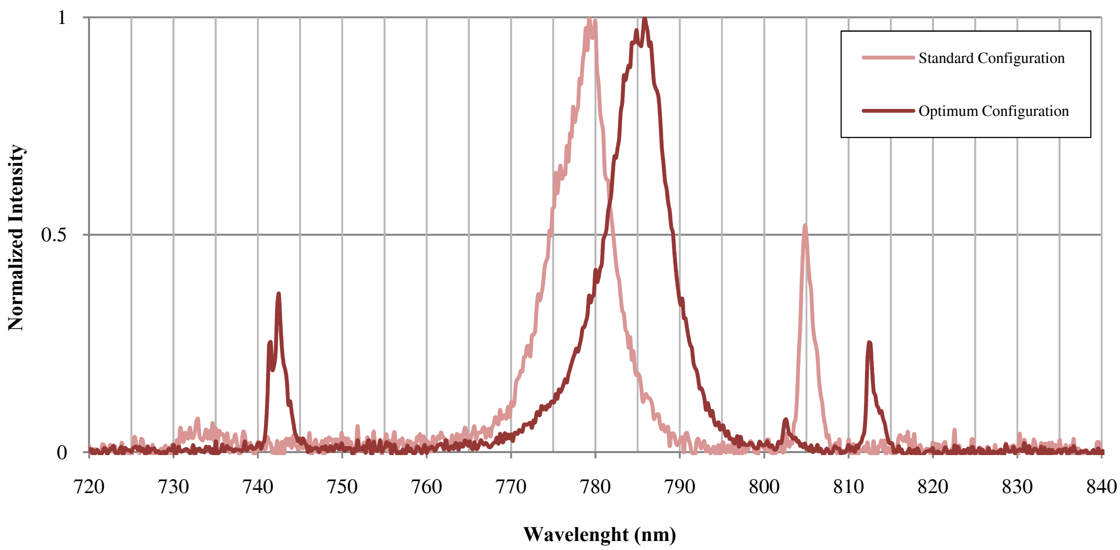

Figure 6-6 - Spectral bandwith of the standard and optimum configuration

6.5 Pulsewidth Measurement

For measuring the pulse width of the optical pulses, we used a Michelson interferometer. (See Appendix II). The autocorrelation measurement for the optimum configuration showed shorter pulsewidth relative to the standard configuration. The pulsewidth for the standard configuration was 112fs and for the optimum configuration it was 76fs. The pulsewidth was determined by assuming a $sech^2$ pulse profile. Figure 6-7 shows the autocorrelation waveform for the optimum configuration.

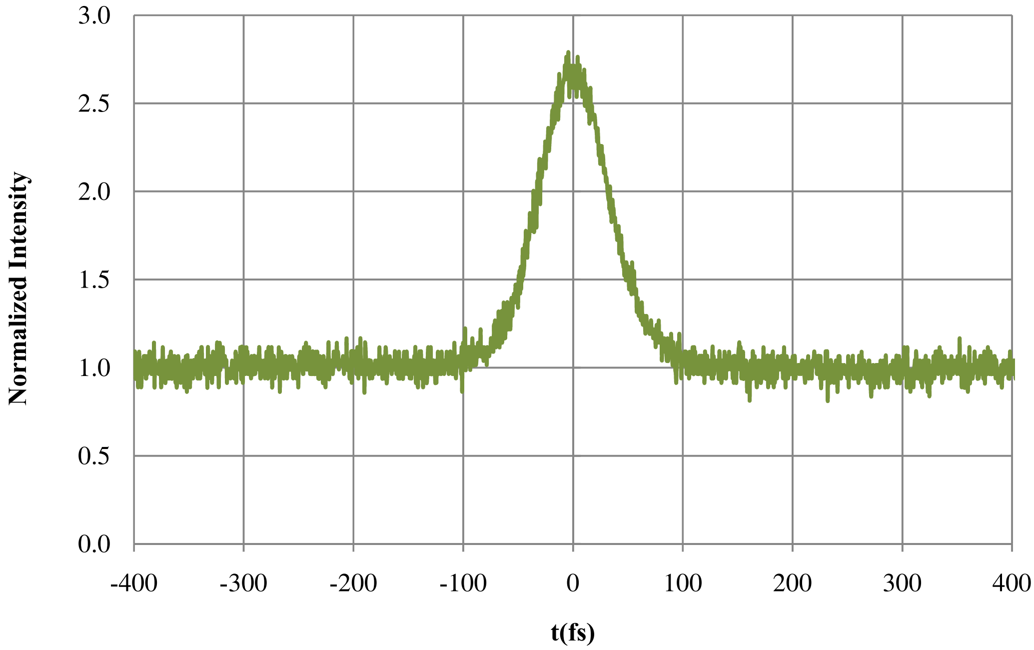

Figure 6-7 - Autocorrelation waveform for optimum configuration

The time-bandwidth product, which is an important parameter for verifying the optical pulse shape is calculated to be about 0.37 for the standard configuration. This is higher than the transform limited value of 0.315 for hyperbolic secant pulses. For the optimum configuration, this parameter was calculated as 0.298, which is lower than the transform-limited value. This is probably due to the fact that, the pulse spectrum shows satellite peaks in addition to the main central band as can be seen in Figure 6.6.

7 Conclusion

In this thesis work, we performed a complete analysis of all loss mechanisms in Multipass-cavity mode-locked lasers to determine the best possible design configuration (having the maximum output pulse energy). Experimentally, a Multipass-cavity Kerr-lens mode-locked Ti:Sapphire laser was constructed using the standard design rules without any clipping losses. The MPC parameters for the initial configuration with negligible clipping loss was m=4 and n=11. In this configuration, the diameter of the beams passing through the notches is slightly smaller than 1/3 of the notch width. The clipping losses for this configuration were calculated to be 1.276×10^{-9} with our simulations. In the KLM operation, 14nJ pulses were generated at a pulse repetition rate of 11.03MHz with an average output power of 156mW at an input pump power of 1.95W.

Using the experimental results of the standard design and detailed modeling of all the clipping losses in the MPC cell, we simulated all realizable configurations. Based on the simulation results, we determined the optimum configuration with m=6 and n=11. For this configuration, we estimated the pulse energy to be around 30nJ, which was 85% higher than the standard configuration.

As one of the adjustable parameters in the MPC design, we also considered the pattern radius on the MPC mirrors and calculated an optimum value for this parameter as well.

Experimental implementation of this configuration showed results which were in very good agreement with our simulations. We measured 32nJ of pulse energy at a pulse repetition rate of 5.80MHz with an average output power of 190mW at the input pump power of 2W. In the experiments, we demonstrated a 101% increase in pulse energy in the optimum configuration relative to the standard configuration. This is within 10% of the theoretical prediction. The horizontally aligned notches in the optimum configuration and the ellipticity in the spot shapes in the MPC cell could be the possible reasons for this discrepancy. Finally, we measured the pulsewidth in the optimum configuration to be 78fs with a spectral width of 8.06nm centered at 786nm.

The theoretical and experimental optimization algorithms developed and tested in this thesis work can be applied to the design of a wide range of femtosecond multi-pass cavity lasers in which notches are employed for beam injection and extraction.

Appendix I: The Knife-Edge Method

The knife-edge method is a simple technique for measuring the spot size of the lowest order Gaussian beams. In this method, a movable blade is positioned perpendicular to the optical axis. It can be shown that the transmitted power in this case is given by[1]

$$T_{edge} = \frac{1}{2}\left(1 + Erf\left(\frac{\sqrt{2}\Delta x}{w}\right)\right), \tag{6.1}$$

where Δx is the distance of the knife-edge from the spot center and w is the spot size. Using this equation, the transmitted power for $\Delta x_1 = -w/2$ and $\Delta x_2 = w/2$, are 0.84 and 0.16. Therefore, if we set the transmission to these values by adjusting the knife position, the corresponding knife positions will be –w/2 and w/2. The difference between these positions is equal to the spot size. Figure A-1 shows the experimental setup for the Knife-edge method.

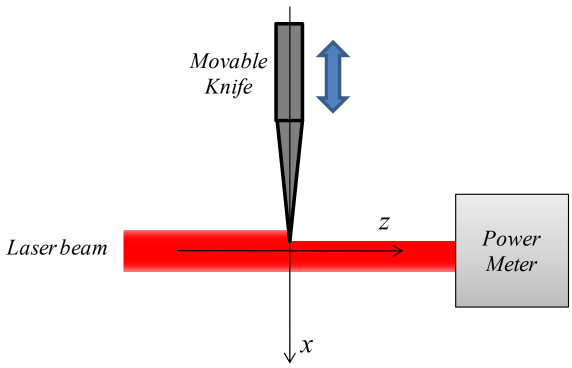

Figure A-1 - Knife-Edge measurment setup

[1] See 4.2.1 for more details.

Appendix II: Autocorrelation Measurement

Measurement of ultra short pulses whose duration is in the femtosecond range is not possible even with the fastest available electronic measurement systems. Measuring these optical pulses is possible with a device known as an autocorrelator. Figure A-2 shows the autocorrelator setup that we used for measuring the pulse durations [30].

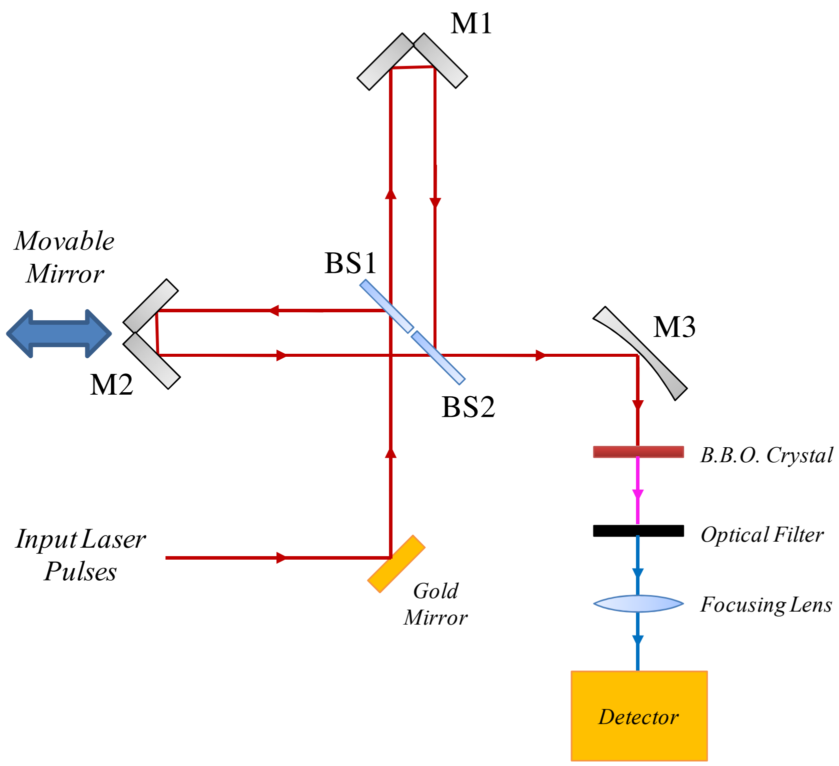

Figure A-2 - Autocorrelator setup

The setup consists of a Michelson interferometer, a non-linear crystal for second harmonic generation and a detector. The movable mirror (M2) in the setup is a corner cube metallic mirror attached to an audio coil actuator. A triangular waveform signal generator with a power amplifier drives the actuator.

The input laser pulse train is split into two pulses by the first beam splitter (BS1). One travels to the movable mirror and the other travels to the fixed mirror (M2). The fixed mirror is also a metallic corner cube mirror. The reflected pulses recombine on the second beam splitter (BS2) and then are focused using a metallic curved mirror (M3) inside the non-linear crystal (BBO crystal in Figure A-2). We used a B.B.O. crystal for second harmonic generation since it has a high conversion efficiency near 800nm [31]. For minimizing the dispersion effect of the crystal, we used a very thin B.B.O. plate of thickness 0.1mm. At the output after strong filtering of the 786nm first harmonic, we used a silicon detector to measure the intensity of the generated second harmonic at 393nm. For a well-aligned system, the peak to background ratio is 3:1 for collinear intensity autocorrelation [32]. Figure A-3 shows the B.B.O. crystal, filters and the generated second harmonic beam. In this photograph, the generated second harmonic beam is visible as a blue spot on a piece of paper placed between the focusing lens and the detector.

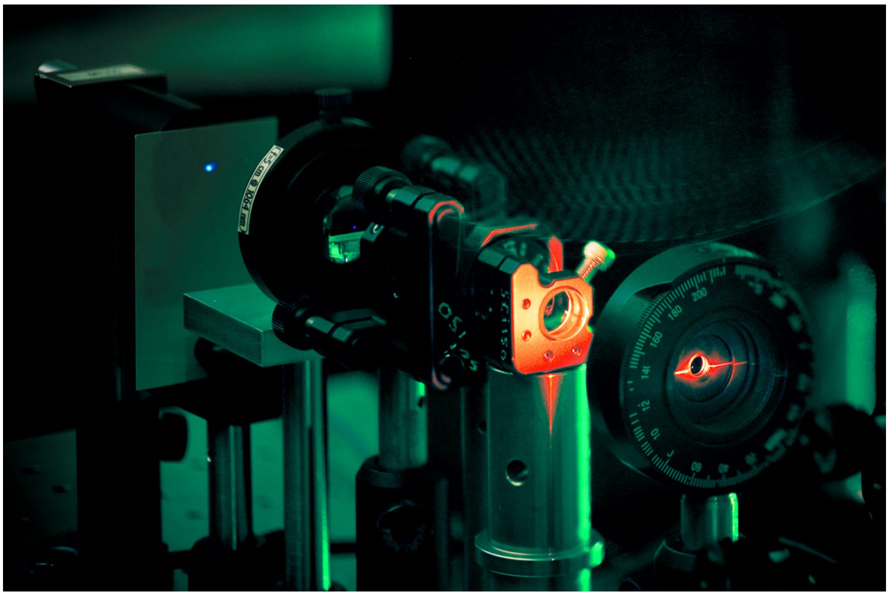

Figure A-3 - Second harmonic generation in the Autocorrelator setup

For measuring the pulsewidth, one must use a slow detector. However, by using a faster detector, it is possible to record the interferometric autocorrelation.

Appendix III: Computer Code

All of the calculation and visualizations in this thesis work are done using Wolfram Mathematica® 7.0 software. Here is the complete code used for doing MPC spot size calculations and pattern sketches.

```
(* MPC Analysis and Pattern Sketch Program *)
(* Aref MostafaZadeh, Aug 25, 2009 - Aug 12, 2010 *)

(* Laser wavelenght *)
λ = 780 * 10^-9;
(* Pump wavelenght *)
λp = 532 * 10^-9;

(* MPC Parameters: *)
R = 2; (* Radius of Curvature of MPC curved mirror *)

(* Initial MPC Configuration *)
n = 11;
m = 4;

(* MPC mirrors radius *)
rmpc = 25.4 * 10^-3;
(* Notch width *)
notch = 5 * 10^-3;

(* Pattern radius on curved mirror *)
rpat = 16 * 10^-3;
```

```
(* Calculating the input beam spot size (beam waist on flat mirror) *)

(* Input beam parameters *)

w1 = 183 * 10^-6; (* Measured beam radius near the waist at z1 *)
w2 = 810 * 10^-6;(* Measured beam radius at distance dz from z1 *)
dz = 0.55;
```

$$\mathrm{wb}[\mathrm{zb\_},\ \lambda\_,\ \mathrm{w0b\_}] := \mathrm{w0b}\sqrt{1+\left(\frac{\lambda\,\mathrm{zb}}{\pi\,\mathrm{w0b}^2}\right)^2};$$

```
NSolve[{wb[z, λ, w] == w1, wb[z + dz, λ, w] == w2}, {z, w}] // EngineeringForm
```

$\{\{z \to -62.2837\times10^{-3},\ w \to 152.206\times10^{-6}\},\ \{z \to 23.1514\times10^{-3},\ w \to 180.198\times10^{-6}\}\}$

```
(* Calculated input beam spot size *)

w0 = 180.198 * 10^-6;
```

```
(* MPC design *)
(* Initial Configuration *)

(* MPC Lenght *)
```

$$\mathrm{dmpc}[\mathrm{n\_},\ \mathrm{m\_},\ \mathrm{r\_}] := \frac{r}{2}\left(1-\mathrm{Cos}\left[\frac{m\,\pi}{n}\right]\right);$$

```
(* MPC Ray Transfer Matrices *)
(* Mirror with radius of curviture r *)
M[r_] := ( 1    0 )
         ( -2/r 1 );

(* Free Space lenght of distance d *)
L[d_] := ( 1 d )
         ( 0 1 );

(* Curved to Curved Unit Cell Matrix *)
Tc[r_, d_] := M[r].L[2 d];

(* Flat to Flat Unit Cell Matrix *)
Tf[r_, d_] := L[d].M[r].L[d];


(* Q-Parameter of the input beam *)
q[0] = - 1/ (ⅈ λ/(π w0^2)) // N

0. + 0.130784 i

qc[0] = q[0];
```

```
(* MPC lenght for Initial Configuration (m) *)
dmpc[n, m, R] // N

0.584585
```

```
(* Pattern radius on the flat mirror (mm) *)
rpatf = rpat Cos[m π/(2 n)] * 10^3 // N

13.4601
```

```
(* Q-Parameter calculations *)

(* Q-Parameter of the first spot on the flat mirror *)

qf1[R_, n_, m_, qi_] := (qi L[dmpc[n, m, R]][[1, 1]] + L[dmpc[n, m, R]][[1, 2]]) /
                        (qi L[dmpc[n, m, R]][[2, 1]] + L[dmpc[n, m, R]][[2, 2]]);

(* Q-Parameter of the Flat Mirror Spots *)
qfi[R_, n_, m_, qi_, i_] :=
 (qf1[R, n, m, qi] MatrixPower[Tf[R, dmpc[n, m, R]], i - 1][[1, 1]] + MatrixPower[Tf[R, dmpc[n, m, R]], i - 1][[
      1, 2]]) / (qf1[R, n, m, qi] MatrixPower[Tf[R, dmpc[n, m, R]], i - 1][[2, 1]] +
    MatrixPower[Tf[R, dmpc[n, m, R]], i - 1][[2, 2]])

(* Q-Parameter of the Curved Mirror Spots *)
qci[R_, n_, m_, qi_, i_] :=
 (qi MatrixPower[Tc[R, dmpc[n, m, R]], i][[1, 1]] + MatrixPower[Tc[R, dmpc[n, m, R]], i][[1, 2]]) /
  (qi MatrixPower[Tc[R, dmpc[n, m, R]], i][[2, 1]] + MatrixPower[Tc[R, dmpc[n, m, R]], i][[2, 2]])
```

```
(* Spot size Calculations *)

w[λ_, q_] := Abs[Sqrt[-λ / (π Im[1 / q])]];

(* Q-Paramter and Spot size for Curved Mirror Spots *)

wf[1] = w[λ, qf1[R, n, m, q[0]]];

For[i = 2, i ≤ n, i++, qf[i] = qfi[R, n, m, q[0], i]; wf[i] = w[λ, qf[i]]]

(* Q-Paramter and Spot size for Curved Mirror Spots *)

For[i = 1, i ≤ n, i++, qc[i] = qci[R, n, m, q[0], i]; wc[i] = w[λ, qc[i]]]

(* Calculation of the Spot Coordinates on MPC mirrors *)

For[i = 1, i ≤ n, i++, θ[i] = (-π i m / n) - π/2; xc[i] = rpat Cos[θ[i]];
 yc[i] = rpat Sin[θ[i]]; xf[i] = rpatf Cos[θ[i]]; yf[i] = rpatf Sin[θ[i]]]
```

```
(* Showing the Numeric Results *)

(* Calculation of Spot Angles in Degrees *)

For[i = 1, i ≤ n, i++,
 θdeg[i] = NumberForm[N[(-(θ[i] + π/2) * 180/π) - (IntegerPart[(-(θ[i] + π/2) * 180/π) / 360] * 360)], 4]]


TableForm[Table[{i, θdeg[i], NumberForm[wc[i] * 10^3, 4], NumberForm[wf[i] * 10^3, 4]}, {i, 1, n}],
 TableHeadings → {{}, {"i     ", "θ(°)   ", "wc(mm) ", "wf(mm)"}}]
```

i	θ(°)	w_c (mm)	w_f (mm)
1	65.45	1.621	0.8254
2	130.9	1.339	1.477
3	196.4	0.5396	0.436
4	261.8	1.759	1.139
5	327.3	0.9616	1.355
6	32.73	0.9811	0.1516
7	98.18	1.755	1.364
8	163.6	0.5183	1.126
9	229.1	1.354	0.4539
10	294.5	1.611	1.479
11	0.	0.1802	0.8089

```
(* Visulisation of the Results *)

(* Distance between mirror sketches *)
gap = rmpc / 2;

(* Display Gamma *)
gamma = 2.2;

(* Pattern radius on the flat mirror *)
rpatf = rpat Cos[m π / (2 n)];

(* Gaussian Beam Intensity Calculations with Display Gamma Correction *)

intensity[x_, y_, x0_, y0_, w_] := (2/(π w^2) e^(-2 ((x-x0)^2 + (y-y0)^2)/w^2))^(1/gamma);
```

```
(* Calculation of the Spot Coordinates on MPC mirrors *)
For[i = 1, i ≤ n, i++, xc[i] = rpat Cos[θ[i]];
 yc[i] = rpat Sin[θ[i]]; xf[i] = rpatf Cos[θ[i]]; yf[i] = rpatf Sin[θ[i]]]

Beam[x0_, y0_, w_] := DensityPlot[intensity[x, y, x0, y0, w], {x, x0 - 2 w, x0 + 2 w},
   {y, y0 - 2 w, y0 + 2 w}, ColorFunction → (RGBColor[1, 0.3, 0, #] &), PlotRange → All, Frame → False];



Show[Graphics[Circle[{0, 0}, rmpc, {ArcSin[notch / (2 rmpc)] - π / 2, 2 π - ArcSin[notch / (2 rmpc)] - π / 2}]],
 Graphics[Line[{{-notch / 2, -rmpc * Cos[notch / (2 rmpc)]}, {-notch / 2, 0}, {notch / 2, 0},
    {notch / 2, -rmpc * Cos[notch / (2 rmpc)]}}]], Graphics[{LightGray, Dashed, Circle[{0, 0}, rpat]}],
 Graphics[{Thick, Red, Dashed, Circle[{xc[1], yc[1]}, wc[1] * 3]}], Table[{Beam[xc[i], yc[i], wc[i]]}, {i, 1, n}],
 Graphics[Table[{Red, Dashed, Circle[{xc[i], yc[i]}, wc[i] * 3]}, {i, 2, n - 1}]],
 Graphics[{Thick, Red, Circle[{xc[n], yc[n]}, wc[n] * 3]}],
 Graphics[{LightGray, Dashed, Circle[{2 rmpc + gap, 0}, rpatf]}],
 Graphics[Circle[{2 rmpc + gap, 0}, rmpc, {ArcSin[notch / (2 rmpc)] - π / 2, 2 π - ArcSin[notch / (2 rmpc)] - π / 2}]],
 Graphics[Line[{{2 rmpc + gap - (notch / 2), -rmpc * Cos[notch / (2 rmpc)]}, {2 rmpc + gap - (notch / 2), 0},
    {2 rmpc + gap + notch / 2, 0}, {2 rmpc + gap + (notch / 2), -rmpc * Cos[notch / (2 rmpc)]}}]],
 Graphics[{Thick, Red, Dashed, Circle[{xf[1] + 2 rmpc + gap, yf[1]}, wf[1] * 3]}],
 Table[{Beam[xf[i] + 2 rmpc + gap, yf[i], wf[i]]}, {i, 1, n}],
 Graphics[Table[{Red, Dashed, Circle[{xf[i] + 2 rmpc + gap, yf[i]}, wf[i] * 3]}, {i, 2, n - 1}]],
 Graphics[{Red, Dashed, Circle[{xf[n] + 2 rmpc + gap, yf[n]}, wf[n] * 3]}],
 Graphics[Text[Style["Curved mirror", Large], {0, -rmpc - (gap / 2)}]],
 Graphics[Text[Style["Flat mirror", Large], {2 rmpc + gap, -rmpc - (gap / 2)}]]]

(* Patterns on the MPC mirrors *)
(* Thick dashed beam is the i=1 case *)
(* Initial Configuration: m=4, n=11 *)
```

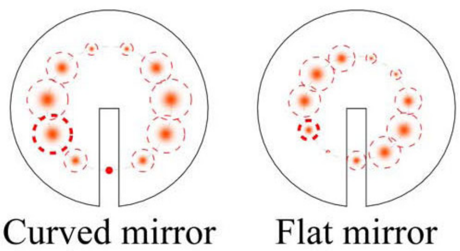


```
(* Left and Right Spot number and Availability Matrices *)
m0 = 2;
n0 = 3;

mmax = 10;
nmax = 50;

(* Zero filling the left spot number matrix *)
Do[LeftSpot[n0, m0] = 0, {m0, 1, mmax}, {n0, 1, nmax}];

(* Left spot number calculation *)
Do[For[i = 1, i ≤ n0, i++, LeftSpot[n0, m0] = If[((π i m0)/n0 - (IntegerPart[(π i m0)/(2 n0 π)] * 2 π) == (2 π)/n0), i, LeftSpot[n0, m0]];
  Break], {n0, m0 + 1, nmax}, {m0, 2, mmax}]

(* Availability matrix *)
Do[Available[n0, m0] = If[LeftSpot[n0, m0] ≠ 0, 1, 0], {m0, 1, mmax}, {n0, 1, nmax}];

(* Right spot number calculation *)
Do[RightSpot[n0, m0] = Available[n0, m0] (n0 - LeftSpot[n0, m0]), {m0, 1, mmax}, {n0, 1, nmax}];
```

```
(* Center Spot Radius of the Flat Mirror *)

Do[InterpolatedPlots[j] = DiscretePlot[w[λ, qfi[R, i, j, q[0], i]] * 1000,
    {i, j + 1, 50, 1}, AxesLabel → {"n", "Center Spot Radius (mm)"}, AspectRatio → 0.5,
    PlotStyle → {RGBColor[j / 10, j / 20, 0], PointSize → 0.006}, Filling → Off, PlotRange → {0, Full},
    AxesOrigin → {0, 0}, Joined → True, InterpolationOrder → 2], {j, 2, 10, 2}];

Do[DiscretePlots[j] = DiscretePlot[w[λ, qfi[R, i, j, q[0], i]] * 1000 * (2 (Available[i, j] - 0.5)), {i, j + 1, 50, 1},
    PlotStyle → {RGBColor[j / 10, j / 20, 0], PointSize → 0.01}, Filling → Off], {j, 2, 10, 2}];

CurrentConfiguration = DiscretePlot[w[λ, qfi[R, n, m, q[0], i]] * 1000,
   {i, n, n}, PlotStyle → {RGBColor[m / 10, m / 20, 0], PointSize → 0.02}, Filling → Off];

PossibleRange = Plot[notch * 167, {i, 0, 50}, Filling → Off, PlotStyle → {Thin, Dashed, Gray}];

Show[InterpolatedPlots[2], InterpolatedPlots[4], InterpolatedPlots[6],
 InterpolatedPlots[8], InterpolatedPlots[10], PossibleRange, DiscretePlots[2],
 DiscretePlots[4], DiscretePlots[6], DiscretePlots[8], DiscretePlots[10], CurrentConfiguration]
```

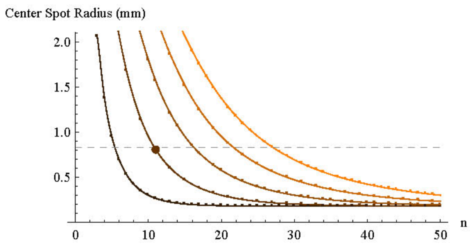


```
(* Clipping Loss Calculations *)
(* Knife-Edge Clipping Losses *)

Tlinear[x_, w_] := 0.5 (1 + Erf[(√2 x)/w]);
```

```
(* Center Spots Clipping Losses *)

TCenterSpots[R_, λ_, n_, m_, qi_, notch_] :=
  (Tlinear[notch / 2, w[λ, qi]]^4) (Tlinear[notch / 2, w[λ, qfi[R, n, m, qi, n]]]^4);

Do[InterpolatedPlots[j] = DiscretePlot[100 * (1 - TCenterSpots[R, λ, i, j, q[0], notch]),
    {i, j + 1, 40}, AxesLabel → {"n", "Center Spot Losses(%)"}, AspectRatio → 0.5,
    PlotStyle → {RGBColor[j / 10, j / 20, 0], PointSize → 0.006}, Filling → Off,
    AxesOrigin → {0, 0}, Joined → True, PlotRange → {0, 13}], {j, 2, 10, 2}];

Do[DiscretePlots[j] = DiscretePlot[100 * (1 - TCenterSpots[R, λ, i, j, q[0], notch]) * (2 (Available[i, j] - 0.5)),
    {i, j + 1, 50, 1}, PlotStyle → {RGBColor[j / 10, j / 20, 0], PointSize → 0.01}, Filling → Off], {j, 2, 10, 2}];

CurrentConfiguration = DiscretePlot[100 * (1 - TCenterSpots[R, λ, i, m, q[0], notch]),
   {i, n, n}, PlotStyle → {RGBColor[m / 10, m / 20, 0], PointSize → 0.02}, Filling → Off];

Show[InterpolatedPlots[2], InterpolatedPlots[4], InterpolatedPlots[6],
 InterpolatedPlots[8], InterpolatedPlots[10], DiscretePlots[2], DiscretePlots[4],
 DiscretePlots[6], DiscretePlots[8], DiscretePlots[10], CurrentConfiguration]
```

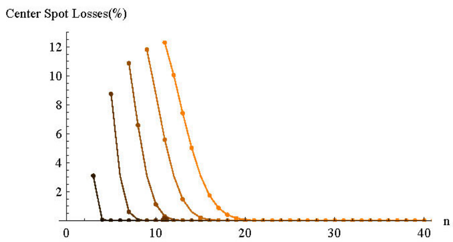

```
(* Side Spots Clipping Losses *)

TSideSpots[R_, λ_, n_, m_, qi_, notch_, rpat_] :=
  Tlinear[Abs[rpat Cos[(m π) / (2 n)] Sin[2 π / n]] - notch / 2, w[λ, qfi[R, n, m, qi, LeftSpot[n, m]]]]^2
   Tlinear[Abs[rpat Cos[(m π) / (2 n)] Sin[2 π / n]] - notch / 2, w[λ, qfi[R, n, m, qi, RightSpot[n, m]]]]^2
   Tlinear[Abs[rpat Sin[2 π / n]] - notch / 2, w[λ, qci[R, n, m, qi, LeftSpot[n, m]]]]^2
   Tlinear[Abs[rpat Sin[2 π / n]] - notch / 2, w[λ, qci[R, n, m, qi, RightSpot[n, m]]]]^2;

InterpolatedPlots[2] = DiscretePlot[100 * (1 - TSideSpots[R, λ, i, 2, q[0], notch, rpat]),
   {i, 3, 50, 1}, AxesLabel → {"n", "Adjacent Spot Losses(%)"},
   AspectRatio → 0.5, PlotStyle → {RGBColor[2 / 10, 2 / 20, 0], PointSize → 0.006},
   Filling → Off, AxesOrigin → {0, 0}, Joined → True, PlotRange → {0, 50}];

InterpolatedPlots[4] = DiscretePlot[100 * (1 - TSideSpots[R, λ, i, 4, q[0], notch, rpat]),
   {i, 5, 50, 2}, AxesLabel → {"n", "Adjacent Spot Losses(%)"},
   AspectRatio → 0.5, PlotStyle → {RGBColor[4 / 10, 4 / 20, 0], PointSize → 0.006},
   Filling → Off, AxesOrigin → {0, 0}, Joined → True, PlotRange → {0, 50}];

InterpolatedPlots[6] = DiscretePlot[100 * (1 - TSideSpots[R, λ, i, 6, q[0], notch, rpat]),
   {i, {7, 8, 10, 11, 13, 14, 16, 17, 19, 20, 22, 23, 25, 26, 28, 29, 31, 32, 34, 35, 37,
     38, 40, 41, 43, 44, 46, 47, 49, 50}}, AxesLabel → {"n", "Adjacent Spot Losses(%)"},
   AspectRatio → 0.5, PlotStyle → {RGBColor[6 / 10, 6 / 20, 0], PointSize → 0.006},
   Filling → Off, AxesOrigin → {0, 0}, Joined → True, PlotRange → {0, 50}];

InterpolatedPlots[8] = DiscretePlot[100 * (1 - TSideSpots[R, λ, i, 8, q[0], notch, rpat]),
   {i, 9, 50, 2}, AxesLabel → {"n", "Adjacent Spot Losses(%)"},
   AspectRatio → 0.5, PlotStyle → {RGBColor[8 / 10, 8 / 20, 0], PointSize → 0.006},
   Filling → Off, AxesOrigin → {0, 0}, Joined → True, PlotRange → {0, 50}];

InterpolatedPlots[10] = DiscretePlot[100 * (1 - TSideSpots[R, λ, i, 10, q[0], notch, rpat]),
   {i, {11, 12, 13, 14, 16, 17, 18, 19, 21, 22, 23, 24, 26, 27, 28, 29, 31, 32}},
   AxesLabel → {"n", "Adjacent Spot Losses(%)"}, AspectRatio → 0.5,
   PlotStyle → {RGBColor[10 / 10, 10 / 20, 0], PointSize → 0.006},
   Filling → Off, AxesOrigin → {0, 0}, Joined → True, PlotRange → {0, 50}];

Do[DiscretePlots[j] =
   DiscretePlot[100 * (1 - TSideSpots[R, λ, i, j, q[0], notch, rpat]) * (2 (Available[i, j] - 0.5)),
    {i, j + 1, 50, 1}, PlotStyle → {RGBColor[j / 10, j / 20, 0], PointSize → 0.01}, Filling → Off], {j, 2, 10, 2}];

CurrentConfiguration = DiscretePlot[100 * (1 - TSideSpots[R, λ, i, m, q[0], notch, rpat]),
   {i, n, n}, PlotStyle → {RGBColor[m / 10, m / 20, 0], PointSize → 0.02}, Filling → Off];

Show[InterpolatedPlots[2], InterpolatedPlots[4], InterpolatedPlots[6],
 InterpolatedPlots[8], InterpolatedPlots[10], DiscretePlots[2], DiscretePlots[4],
 DiscretePlots[6], DiscretePlots[8], DiscretePlots[10], CurrentConfiguration]
```

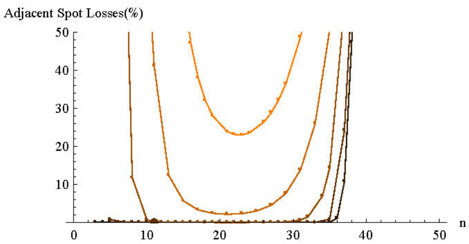

```
(* Surface Clipping Losses *)

TRadial[R_, λ_, n_, m_, qi_, rmpc_, rpat_] := Product[Tlinear[rmpc - rpat, w[λ, qci[R, n, m, qi, k]]]^2, {k, 1, n - 1}]
   Product[Tlinear[rmpc - (rpat Cos[(m π) / (2 n)]), w[λ, qfi[R, n, m, qi, k]]]^2, {k, 1, n - 1}];

Do[InterpolatedPlots[j] = DiscretePlot[100 * (1 - TRadial[R, λ, i, j, q[0], rmpc, rpat]),
    {i, j + 1, 50, 1}, AxesLabel → {"n", "Surface Clipping Losses(%)"}, AspectRatio → 0.5,
    PlotStyle → {RGBColor[j / 10, j / 20, 0], PointSize → 0.006}, Filling → Off,
    AxesOrigin → {0, 0}, Joined → True, PlotRange → {0, 90}], {j, 2, 10, 2}];

Do[DiscretePlots[j] = DiscretePlot[100 * (1 - TRadial[R, λ, i, j, q[0], rmpc, rpat]) * (2 (Available[i, j] - 0.5)),
    {i, j + 1, 50, 1}, PlotStyle → {RGBColor[j / 10, j / 20, 0], PointSize → 0.01}, Filling → Off], {j, 2, 10, 2}];

CurrentConfiguration = DiscretePlot[100 * (1 - TRadial[R, λ, i, m, q[0], rmpc, rpat]),
   {i, n, n}, PlotStyle → {RGBColor[m / 10, m / 20, 0], PointSize → 0.02}, Filling → Off];

Show[InterpolatedPlots[2], InterpolatedPlots[4], InterpolatedPlots[6],
 InterpolatedPlots[8], InterpolatedPlots[10], DiscretePlots[2], DiscretePlots[4],
 DiscretePlots[6], DiscretePlots[8], DiscretePlots[10], CurrentConfiguration]
```

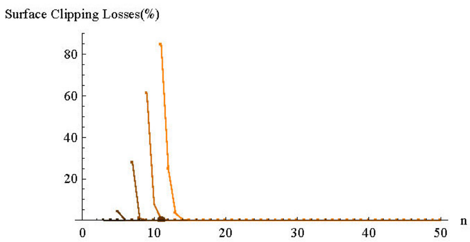


```
(* Total Clipping Losses *)

TClipping[R_, λ_, n_, m_, qi_, rmpc_, rpat_, notch_] :=
  TCenterSpots[R, λ, n, m, qi, notch] TSideSpots[R, λ, n, m, qi, notch, rpat] TRadial[R, λ, n, m, qi, rmpc, rpat];

InterpolatedPlots[2] = DiscretePlot[100 * (1 - TClipping[R, λ, i, 2, q[0], rmpc, rpat, notch]),
   {i, 3, 50, 1}, AxesLabel → {"n", "Total Clipping Losses(%)"},
   AspectRatio → 0.5, PlotStyle → {RGBColor[2 / 10, 2 / 20, 0], PointSize → 0.006},
   Filling → Off, AxesOrigin → {0, 0}, Joined → True, PlotRange → {0, 50}];

InterpolatedPlots[4] = DiscretePlot[100 * (1 - TClipping[R, λ, i, 4, q[0], rmpc, rpat, notch]),
   {i, 5, 50, 2}, PlotStyle → {RGBColor[4 / 10, 4 / 20, 0], PointSize → 0.006},
   Filling → Off, AxesOrigin → {0, 0}, Joined → True, PlotRange → {0, 50}];

InterpolatedPlots[6] = DiscretePlot[100 * (1 - TClipping[R, λ, i, 6, q[0], rmpc, rpat, notch]),
   {i, {7, 8, 10, 11, 13, 14, 16, 17, 19, 20, 22, 23, 25, 26, 28, 29, 31, 32, 34, 35, 37, 38, 40,
     41, 43, 44, 46, 47, 49, 50}}, PlotStyle → {RGBColor[6 / 10, 6 / 20, 0], PointSize → 0.006},
   Filling → Off, AxesOrigin → {0, 0}, Joined → True, PlotRange → {0, 50}];

InterpolatedPlots[8] = DiscretePlot[100 * (1 - TClipping[R, λ, i, 8, q[0], rmpc, rpat, notch]),
   {i, 9, 50, 2}, PlotStyle → {RGBColor[8 / 10, 8 / 20, 0], PointSize → 0.006},
   Filling → Off, AxesOrigin → {0, 0}, Joined → True, PlotRange → {0, 50}];

InterpolatedPlots[10] = DiscretePlot[100 * (1 - TClipping[R, λ, i, 10, q[0], rmpc, rpat, notch]),
   {i, {11, 12, 13, 14, 16, 17, 18, 19, 21, 22, 23, 24, 26, 27, 28, 29, 31, 32}},
   PlotStyle → {RGBColor[10 / 10, 10 / 20, 0], PointSize → 0.006},
   Filling → Off, AxesOrigin → {0, 0}, Joined → True, PlotRange → {0, 50}];

Do[DiscretePlots[j] =
   DiscretePlot[100 * (1 - TClipping[R, λ, i, j, q[0], rmpc, rpat, notch]) * (2 (Available[i, j] - 0.5)),
    {i, j + 1, 50, 1}, PlotStyle → {RGBColor[j / 10, j / 20, 0], PointSize → 0.01}, Filling → Off], {j, 2, 10, 2}];

CurrentConfiguration = DiscretePlot[100 * (1 - TClipping[R, λ, i, m, q[0], rmpc, rpat, notch]),
   {i, n, n}, PlotStyle → {RGBColor[m / 10, m / 20, 0], PointSize → 0.02}, Filling → Off];
```

```
Show[InterpolatedPlots[2], InterpolatedPlots[4], InterpolatedPlots[6],
 InterpolatedPlots[8], InterpolatedPlots[10], DiscretePlots[2], DiscretePlots[4],
 DiscretePlots[6], DiscretePlots[8], DiscretePlots[10], CurrentConfiguration]
```

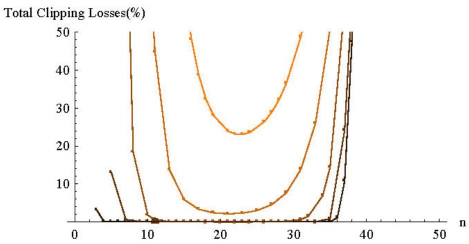


```
(* Total Clipping Loss Values *)

TableForm[{{ScientificForm[1 - TCenterSpots[R, λ, n, m, q[0], notch]], ScientificForm[
    1 - TSideSpots[R, λ, n, m, q[0], notch, rpat]], ScientificForm[1 - TRadial[R, λ, n, m, q[0], rmpc, rpat]]},
  {}, {NumberForm[(1 - TClipping[R, λ, n, m, q[0], rmpc, rpat, notch]) * 100, 4]}},
 TableHeadings → {{StringJoin[{"For m=", ToString[m], ", n=", ToString[n]}], "", "Total Clipping Loses(%):"},
   {"Center Spot Losses  ", "Adjacent Spots Losses  ", "Surface Losses"}}]
```

	Center Spot Losses	Adjacent Spots Losses	Surface Losses
For m=4, n=11	1.27378×10^{-9}	1.80522×10^{-12}	0.
Total Clipping Loses(%):	1.276×10^{-7}		

```
(* Output Power and Pulse Energy Analysis *)

(* Input pump power before lens in Watts *)
pin = 1.95;

 (* Transmision of the optics before Crystal *)
tin = 0.93;

(* Incident pump power on crystal *)
pp = pin tin;

(* Short cavity threshold power *)
pthsh = 167 * 10^-3;

(* CW Pump threshold power with MPC *)
pthmpc = 264 * 10^-3;

(* KLM Pump threshold power based on KLM slope efficiency trendline
 calculation (Measured CW thereshold with in KLM operation point was 492mW *)
pthklm = 540 * 10^-3;

(* Output coupler transmision *)
toc = 3 * 10^-2;

(* Additional GTI mirrors reflection coefficient *)
tgti = 0.998;

(* Short cavity lenght *)
d0 = 72.2 * 10^-2;

(* Short arm measured laser slope efficiency *)
seffsh = 0.253;

(* MPC CW Measured laser slope efficiency *)
seffmpc = 0.1486;

(* MPC Pulsed Measured laser slope efficiency *)
seffklm = 0.1233;
```

```
(* Fractional power absorbtion *)
η = 0.74;

(* Total MPC loss (Reflection + Clipping Loses) *)

Tmpc[tmpcmirror_, tgti_, R_, λ_, n_, m_, qi_, rmpc_, rpat_, notch_] :=
  tmpcmirror^(4 (n-1)) (TClipping[R, λ, n, m, qi, rmpc, rpat, notch]) tgti^4;

(* Tatal Cavity Loss *)

Trans[t0_, tmpcmirror_, tgti_, R_, λ_, n_, m_, qi_, rmpc_, rpat_, notch_] :=
  t0 Tmpc[tmpcmirror, tgti, R, λ, n, m, qi, rmpc, rpat, notch];

(* Threshold Power *)

pthr[a_, t0_, tmpcmirror_, tgti_, toc_, R_, λ_, n_, m_, qi_, rmpc_, rpat_, notch_] :=
  a (1 - (Trans[t0, tmpcmirror, tgti, R, λ, n, m, qi, rmpc, rpat, notch] (1 - toc)));

(* Slope Efficiency *)

seff[λp_, toc_, t0_, tmpcmirror_, tgti_, η_, R_, λ_, n_, m_, qi_, rmpc_, rpat_, notch_] :=
  λp/λ (toc / (1 - (Trans[t0, tmpcmirror, tgti, R, λ, n, m, qi, rmpc, rpat, notch] (1 - toc)))) η;

(* Short Cavity Efficiency *)
seffshort[λp_, λ_, toc_, t0_, η_] := λp/λ (toc / (1 - (t0 (1 - toc)))) η;

(* Output Power *)

pout[pp_, λp_, a_, toc_, t0_, tmpcmirror_, tgti_, η_, R_, λ_, n_, m_, qi_, rmpc_, rpat_, notch_] :=
  seff[λp, toc, t0, tmpcmirror, tgti, η, R, λ, n, m, qi, rmpc, rpat, notch]
   (pp - pthr[a, t0, tmpcmirror, tgti, toc, R, λ, n, m, qi, rmpc, rpat, notch]);

(* Repetution rate frequency *)

frep[d0_, n_, m_, R_] := 2.99792458 * 10^8 / (2 d0 + 4 n dmpc[n, m, R]);

(* Pulse Energy *)

PulseEnergy[pp_, λp_, a_, toc_, t0_, tmpcmirror_, tgti_, d0_, η_, R_, λ_, n_, m_, qi_, rmpc_, rpat_, notch_] :=
  pout[pp, λp, a, toc, t0, tmpcmirror, tgti, η, R, λ, n, m, qi, rmpc, rpat, notch] / frep[d0, n, m, R];

NSolve[seffshort[λp, λ, toc, x, η] == seffsh, x]
{{x → 0.969229}}

t0 = 0.969229;(* Calculated value based on slope efficiency equation *)

(* Short Cavity Lose *)
(1 - t0 ) * 100
3.0771

FindRoot[seff[λp, toc, t0, x, tgti, η, R, λ, n, m, q[0], rmpc, rpat, notch] == seffklm, {x, 0.001}]
{x → 0.998469}

tmpcmirror = 0.998469;(* Calculated value based on slope efficiency equation *)

NSolve[{pthr[x, t0, tmpcmirror, tgti, toc, R, λ, n, m, q[0], rmpc, rpat, notch] == pthklm}, {x}]
{{x → 4.39776}}

a = 4.39776; (* Calculated based on calculated KLM threshold power *)
```

```
(* Total Losses Including Reflection Losses *)

InterpolatedPlots[2] = DiscretePlot[(1 - Trans[t0, tmpcmirror, tgti, R, λ, i, 2, q[0], rmpc, rpat, notch]) * 100,
   {i, 3, 50, 1}, AxesLabel → {"n", "Total Losses(%)"}, AspectRatio → 0.5,
   PlotStyle → {RGBColor[2 / 10, 2 / 20, 0], PointSize → 0.006},
   Filling → Off, AxesOrigin → {0, 0}, Joined → True, PlotRange → {0, 102}];

InterpolatedPlots[4] = DiscretePlot[(1 - Trans[t0, tmpcmirror, tgti, R, λ, i, 4, q[0], rmpc, rpat, notch]) * 100,
   {i, 5, 50, 2}, PlotStyle → {RGBColor[4 / 10, 4 / 20, 0], PointSize → 0.006},
   Filling → Off, AxesOrigin → {0, 0}, Joined → True, PlotRange → {0, 100}];

InterpolatedPlots[6] = DiscretePlot[(1 - Trans[t0, tmpcmirror, tgti, R, λ, i, 6, q[0], rmpc, rpat, notch]) * 100,
   {i, {7, 8, 10, 11, 13, 14, 16, 17, 19, 20, 22, 23, 25, 26, 28, 29, 31, 32, 34, 35, 37, 38, 40,
     41, 43, 44, 46, 47, 49, 50}}, PlotStyle → {RGBColor[6 / 10, 6 / 20, 0], PointSize → 0.006},
   Filling → Off, AxesOrigin → {0, 0}, Joined → True, PlotRange → {0, 100}];

InterpolatedPlots[8] = DiscretePlot[(1 - Trans[t0, tmpcmirror, tgti, R, λ, i, 8, q[0], rmpc, rpat, notch]) * 100,
   {i, 9, 50, 2}, PlotStyle → {RGBColor[8 / 10, 8 / 20, 0], PointSize → 0.006},
   Filling → Off, AxesOrigin → {0, 0}, Joined → True, PlotRange → {0, 100}];

InterpolatedPlots[10] = DiscretePlot[(1 - Trans[t0, tmpcmirror, tgti, R, λ, i, 10, q[0], rmpc, rpat, notch]) * 100,
   {i, {11, 12, 13, 14, 16, 17, 18, 19, 21, 22, 23, 24, 26, 27, 28, 29, 31, 32, 33, 34, 36, 37, 38, 39,
     41, 42, 43, 44, 46, 47, 48, 49}}, PlotStyle → {RGBColor[10 / 10, 10 / 20, 0], PointSize → 0.006},
   Filling → Off, AxesOrigin → {0, 0}, Joined → True, PlotRange → {0, 100}];

Do[DiscretePlots[j] = DiscretePlot[
    (1 - Trans[t0, tmpcmirror, tgti, R, λ, i, j, q[0], rmpc, rpat, notch]) * 100 * (2 (Available[i, j] - 0.5)),
    {i, j + 1, 50, 1}, PlotStyle → {RGBColor[j / 10, j / 20, 0], PointSize → 0.01}, Filling → Off], {j, 2, 10, 2}];

CurrentConfiguration = DiscretePlot[(1 - Trans[t0, tmpcmirror, tgti, R, λ, i, m, q[0], rmpc, rpat, notch]) * 100,
   {i, n, n}, PlotStyle → {RGBColor[m / 10, m / 20, 0], PointSize → 0.02}, Filling → Off];

Show[InterpolatedPlots[2], InterpolatedPlots[4], InterpolatedPlots[6],
 InterpolatedPlots[8], InterpolatedPlots[10], DiscretePlots[2], DiscretePlots[4],
 DiscretePlots[6], DiscretePlots[8], DiscretePlots[10], CurrentConfiguration]
```

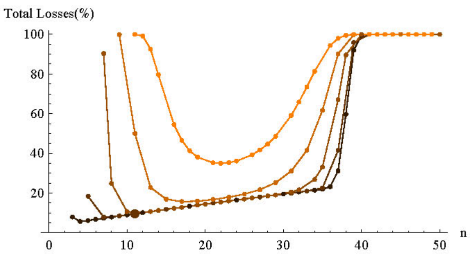


```
(* Average Output Power *)

InterpolatedPlots[2] =
  DiscretePlot[pout[pp, λp, a, toc, t0, tmpcmirror, tgti, η, R, λ, i, 2, q[0], rmpc, rpat, notch] * 1000,
   {i, 3, 50, 1}, AxesLabel → {"n", "Output Power(mW)"}, AspectRatio → 0.5,
   PlotStyle → {RGBColor[2 / 10, 2 / 20, 0], PointSize → 0.006},
   Filling → Off, AxesOrigin → {0, 0}, Joined → True, PlotRange → {0, 300}];

InterpolatedPlots[4] = DiscretePlot[
   pout[pp, λp, a, toc, t0, tmpcmirror, tgti, η, R, λ, i, 4, q[0], rmpc, rpat, notch] * 1000, {i, 5, 50, 2},
   PlotStyle → {RGBColor[4 / 10, 4 / 20, 0], PointSize → 0.006}, Filling → Off, AxesOrigin → {0, 0}, Joined → True];

InterpolatedPlots[6] = DiscretePlot[
   pout[pp, λp, a, toc, t0, tmpcmirror, tgti, η, R, λ, i, 6, q[0], rmpc, rpat, notch] * 1000, {i, {7, 8, 10, 11,
     13, 14, 16, 17, 19, 20, 22, 23, 25, 26, 28, 29, 31, 32, 34, 35, 37, 38, 40, 41, 43, 44, 46, 47, 49, 50}},
   PlotStyle → {RGBColor[6 / 10, 6 / 20, 0], PointSize → 0.006}, Filling → Off, AxesOrigin → {0, 0}, Joined → True];

InterpolatedPlots[8] = DiscretePlot[
   pout[pp, λp, a, toc, t0, tmpcmirror, tgti, η, R, λ, i, 8, q[0], rmpc, rpat, notch] * 1000, {i, 9, 50, 2},
   PlotStyle → {RGBColor[8 / 10, 8 / 20, 0], PointSize → 0.006}, Filling → Off, AxesOrigin → {0, 0}, Joined → True];
```

```
InterpolatedPlots[10] =
  DiscretePlot[pout[pp, λp, a, toc, t0, tmpcmirror, tgti, η, R, λ, i, 10, q[0], rmpc, rpat, notch] * 1000,
   {i, {11, 12, 13, 14, 16, 17, 18, 19, 21, 22, 23, 24, 26, 27, 28, 29, 31,
     32, 33, 34, 36, 37, 38, 39, 41, 42, 43, 44, 46, 47, 48, 49}}, PlotStyle →
    {RGBColor[10 / 10, 10 / 20, 0], PointSize → 0.006}, Filling → Off, AxesOrigin → {0, 0}, Joined → True];

Do[DiscretePlots[j] = DiscretePlot[If[2 (Available[i, j] - 0.5) > 0,
     pout[pp, λp, a, toc, t0, tmpcmirror, tgti, η, R, λ, i, j, q[0], rmpc, rpat, notch] * 1000, -1],
    {i, j + 1, 50, 1}, PlotStyle → {RGBColor[j / 10, j / 20, 0], PointSize → 0.01}, Filling → Off], {j, 2, 10, 2}];

CurrentConfiguration =
  DiscretePlot[pout[pp, λp, a, toc, t0, tmpcmirror, tgti, η, R, λ, i, m, q[0], rmpc, rpat, notch] * 1000,
   {i, n, n}, PlotStyle → {RGBColor[m / 10, m / 20, 0], PointSize → 0.02}, Filling → Off];

Show[InterpolatedPlots[2], InterpolatedPlots[4], InterpolatedPlots[6],
 InterpolatedPlots[8], InterpolatedPlots[10], DiscretePlots[2], DiscretePlots[4],
 DiscretePlots[6], DiscretePlots[8], DiscretePlots[10], CurrentConfiguration]
```

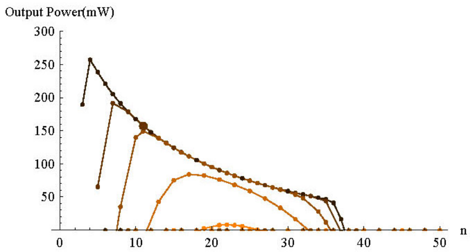


```
(* Output Power for Current Configuration *)
pout[2, λp, a, toc, t0, tmpcmirror, tgti, η, R, λ, n, 4, q[0], rmpc, rpat, notch] // EngineeringForm
```

180.037×10^{-3}

```
frep[d0, n, 4, R] // EngineeringForm
```

11.0357×10^{6}

```
(* MPC Lenght *)

InterpolatedPlots[2] = DiscretePlot[dmpc[i, 2, R], {i, 3, 50, 1}, AxesLabel → {"n", "MPC Lenght (m)"},
   AspectRatio → 0.5, PlotStyle → {RGBColor[2 / 10, 2 / 20, 0], PointSize → 0.006},
   Filling → Off, AxesOrigin → {0, 0}, Joined → True, PlotRange → {0, 2}];

InterpolatedPlots[4] = DiscretePlot[dmpc[i, 4, R], {i, 5, 50, 2},
   PlotStyle → {RGBColor[4 / 10, 4 / 20, 0], PointSize → 0.006}, Filling → Off, AxesOrigin → {0, 0}, Joined → True];

InterpolatedPlots[6] = DiscretePlot[dmpc[i, 6, R], {i, {7, 8, 10, 11, 13, 14, 16,
     17, 19, 20, 22, 23, 25, 26, 28, 29, 31, 32, 34, 35, 37, 38, 40, 41, 43, 44, 46, 47, 49, 50}},
   PlotStyle → {RGBColor[6 / 10, 6 / 20, 0], PointSize → 0.006}, Filling → Off, AxesOrigin → {0, 0}, Joined → True];

InterpolatedPlots[8] = DiscretePlot[dmpc[i, 8, R], {i, 9, 50, 2},
   PlotStyle → {RGBColor[8 / 10, 8 / 20, 0], PointSize → 0.006}, Filling → Off, AxesOrigin → {0, 0}, Joined → True];

InterpolatedPlots[10] =
  DiscretePlot[dmpc[i, 10, R], {i, {11, 12, 13, 14, 16, 17, 18, 19, 21, 22, 23, 24, 26, 27, 28,
     29, 31, 32, 33, 34, 36, 37, 38, 39, 41, 42, 43, 44, 46, 47, 48, 49}}, PlotStyle →
    {RGBColor[10 / 10, 10 / 20, 0], PointSize → 0.006}, Filling → Off, AxesOrigin → {0, 0}, Joined → True];

Do[DiscretePlots[j] = DiscretePlot[If[2 (Available[i, j] - 0.5) > 0, dmpc[i, j, R], -0.1], {i, j + 1, 50, 1},
    PlotStyle → {RGBColor[j / 10, j / 20, 0], PointSize → 0.01}, Filling → Off, AxesLabel →
     {"n", "Total Cavity Lenght (m)"}, AspectRatio → 0.5, AxesOrigin → {0, 0}, PlotRange → {0, 3}], {j, 2, 10, 2}];

CurrentConfiguration = DiscretePlot[dmpc[i, m, R], {i, n, n},
   PlotStyle → {RGBColor[m / 10, m / 20, 0], PointSize → 0.02}, Filling → Off];
```

```
Show[InterpolatedPlots[2], InterpolatedPlots[4], InterpolatedPlots[6],
 InterpolatedPlots[8], InterpolatedPlots[10], DiscretePlots[2], DiscretePlots[4],
 DiscretePlots[6], DiscretePlots[8], DiscretePlots[10], CurrentConfiguration]
```

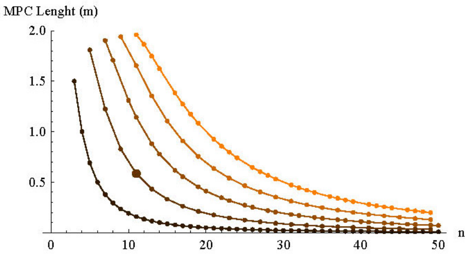

```
(* Total Cavity Lenght *)

InterpolatedPlots[2] =
  DiscretePlot[2 (i * dmpc[i, 2, R] + d0), {i, 3, 50, 1}, AxesLabel → {"n", "Total Cavity Lenght (m)"},
   AspectRatio → 0.5, PlotStyle → {RGBColor[2 / 10, 2 / 20, 0], PointSize → 0.006},
   Filling → Off, AxesOrigin → {0, 0}, Joined → True, PlotRange → {0, 50}];

InterpolatedPlots[4] = DiscretePlot[2 (i * dmpc[i, 4, R] + d0), {i, 5, 50, 2},
   PlotStyle → {RGBColor[4 / 10, 4 / 20, 0], PointSize → 0.006}, Filling → Off, AxesOrigin → {0, 0}, Joined → True];

InterpolatedPlots[6] = DiscretePlot[2 (i * dmpc[i, 6, R] + d0), {i, {7, 8, 10, 11, 13, 14,
     16, 17, 19, 20, 22, 23, 25, 26, 28, 29, 31, 32, 34, 35, 37, 38, 40, 41, 43, 44, 46, 47, 49, 50}},
   PlotStyle → {RGBColor[6 / 10, 6 / 20, 0], PointSize → 0.006}, Filling → Off, AxesOrigin → {0, 0}, Joined → True];

InterpolatedPlots[8] = DiscretePlot[2 (i * dmpc[i, 8, R] + d0), {i, 9, 50, 2},
   PlotStyle → {RGBColor[8 / 10, 8 / 20, 0], PointSize → 0.006}, Filling → Off, AxesOrigin → {0, 0}, Joined → True];

InterpolatedPlots[10] =
  DiscretePlot[2 (i * dmpc[i, 10, R] + d0), {i, {11, 12, 13, 14, 16, 17, 18, 19, 21, 22, 23, 24,
     26, 27, 28, 29, 31, 32, 33, 34, 36, 37, 38, 39, 41, 42, 43, 44, 46, 47, 48, 49}}, PlotStyle →
    {RGBColor[10 / 10, 10 / 20, 0], PointSize → 0.006}, Filling → Off, AxesOrigin → {0, 0}, Joined → True];

Do[DiscretePlots[j] = DiscretePlot[If[2 (Available[i, j] - 0.5) > 0, 2 (i * dmpc[i, j, R] + d0), -1],
    {i, j + 1, 50, 1}, PlotStyle → {RGBColor[j / 10, j / 20, 0], PointSize → 0.01}, Filling → Off, AxesLabel →
     {"n", "Total Cavity Lenght (m)"}, AspectRatio → 0.5, AxesOrigin → {0, 0}, PlotRange → {0, 3}], {j, 2, 10, 2}];

CurrentConfiguration = DiscretePlot[2 (i * dmpc[i, m, R] + d0),
   {i, n, n}, PlotStyle → {RGBColor[m / 10, m / 20, 0], PointSize → 0.02}, Filling → Off];

Show[InterpolatedPlots[2], InterpolatedPlots[4], InterpolatedPlots[6],
 InterpolatedPlots[8], InterpolatedPlots[10], DiscretePlots[2], DiscretePlots[4],
 DiscretePlots[6], DiscretePlots[8], DiscretePlots[10], CurrentConfiguration]
```

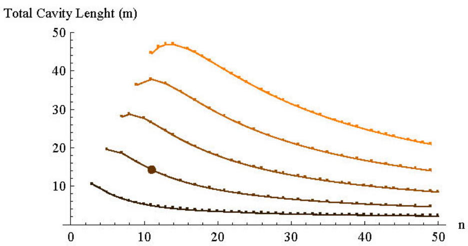

```
(* Pulse Energy *)

InterpolatedPlots[2] = DiscretePlot[
   PulseEnergy[pp, λp, a, toc, t0, tmpcmirror, tgti, d0, η, R, λ, i, 2, q[0], rmpc, rpat, notch] * 10^9,
   {i, 3, 50, 1}, AxesLabel → {"n", "Pulse Energy (nJ)"}, AspectRatio → 0.5,
   PlotStyle → {RGBColor[2 / 10, 2 / 20, 0], PointSize → 0.01},
   Filling → Off, AxesOrigin → {0, 0}, Joined → True, PlotRange → {0, 30}];

InterpolatedPlots[4] = DiscretePlot[
   PulseEnergy[pp, λp, a, toc, t0, tmpcmirror, tgti, d0, η, R, λ, i, 4, q[0], rmpc, rpat, notch] * 10^9,
   {i, 5, 50, 2}, PlotStyle → {RGBColor[4 / 10, 4 / 20, 0], PointSize → 0.01},
   Filling → Off, AxesOrigin → {0, 0}, Joined → True];

InterpolatedPlots[6] = DiscretePlot[
   PulseEnergy[pp, λp, a, toc, t0, tmpcmirror, tgti, d0, η, R, λ, i, 6, q[0], rmpc, rpat, notch] * 10^9, {i, {7, 8,
     10, 11, 13, 14, 16, 17, 19, 20, 22, 23, 25, 26, 28, 29, 31, 32, 34, 35, 37, 38, 40, 41, 43, 44, 46, 47, 49, 50}},
   PlotStyle → {RGBColor[6 / 10, 6 / 20, 0], PointSize → 0.01}, Filling → Off, AxesOrigin → {0, 0}, Joined → True];

InterpolatedPlots[8] = DiscretePlot[
   PulseEnergy[pp, λp, a, toc, t0, tmpcmirror, tgti, d0, η, R, λ, i, 8, q[0], rmpc, rpat, notch] * 10^9,
   {i, 9, 50, 2}, PlotStyle → {RGBColor[8 / 10, 8 / 20, 0], PointSize → 0.01},
   Filling → Off, AxesOrigin → {0, 0}, Joined → True];

InterpolatedPlots[10] = DiscretePlot[
   PulseEnergy[pp, λp, a, toc, t0, tmpcmirror, tgti, d0, η, R, λ, i, 10, q[0], rmpc, rpat, notch] * 10^9,
   {i, {11, 12, 13, 14, 16, 17, 18, 19, 21, 22, 23, 24, 26, 27, 28, 29, 31,
     32, 33, 34, 36, 37, 38, 39, 41, 42, 43, 44, 46, 47, 48, 49}}, PlotStyle →
    {RGBColor[10 / 10, 10 / 20, 0], PointSize → 0.01}, Filling → Off, AxesOrigin → {0, 0}, Joined → True];

Do[DiscretePlots[j] =
   DiscretePlot[If[2 (Available[i, j] - 0.5) > 0, PulseEnergy[pp, λp, a, toc, t0, tmpcmirror, tgti,
       d0, η, R, λ, i, j, q[0], rmpc, rpat, notch] * 10^9, -1 * 10^9], {i, j + 1, 50, 1},
    PlotStyle → {RGBColor[j / 10, j / 20, 0], PointSize → 0.01}, Filling → Off], {j, 2, 10, 2}];

CurrentConfiguration = DiscretePlot[
   PulseEnergy[pp, λp, a, toc, t0, tmpcmirror, tgti, d0, η, R, λ, i, m, q[0], rmpc, rpat, notch] * 10^9,
   {i, n, n}, PlotStyle → {RGBColor[m / 10, m / 20, 0], PointSize → 0.02}, Filling → Off];

Show[InterpolatedPlots[2], InterpolatedPlots[4], InterpolatedPlots[6],
 InterpolatedPlots[8], InterpolatedPlots[10], DiscretePlots[2], DiscretePlots[4],
 DiscretePlots[6], DiscretePlots[8], DiscretePlots[10], CurrentConfiguration]
```

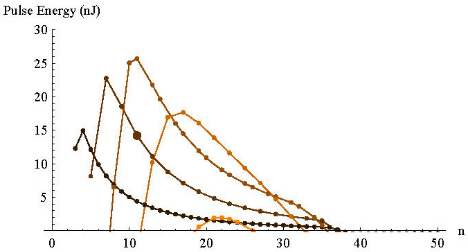


```
PulseEnergy[2, λp, a, toc, t0, tmpcmirror, tgti, d0, η, R, λ, n, 6, q[0], rmpc, rpat, notch] // EngineeringForm
```

29.5433×10^{-9}

```
2 (n * dmpc[n, 6, R] + d0)
```

26.5749

```
(* Optimum Configuration *)
mopt = 6;
nopt = 11;

m = 4;
```

```
(* Optimum MPC Lenght *)
dmpc[nopt, mopt, R] // N

1.14231

(* Repetition Rate for Optimum Configuration *)
frep[d0, nopt, mopt, R]

5.79804 × 10^6

(* Pulse Enrgy in Optimum Configuration *)
PulseEnergy[pp, λp, a, toc, t0, tmpcmirror, tgti,
  d0, η, R, λ, nopt, mopt, q[0], rmpc, rpat, notch] // EngineeringForm

26.6713 × 10^-9

(* Pulse energy increase in optimized configuration in percents (%) *)
((PulseEnergy[pp, λp, a, toc, t0, tmpcmirror, tgti, d0, η, R, λ, nopt, mopt, q[0], rmpc, rpat, notch] /
      PulseEnergy[pp, λp, a, toc, t0, tmpcmirror, tgti, d0, η, R, λ, n, m, q[0], rmpc, rpat, notch]) - 1) * 100 // N

80.8264
```

```
(* Optimum Pattern Radius in Optimum Configuration *)
(* Plotting the Clipping Losses as a Function of the Pattern Radius on Curved Mirror *)

Plot[{(1 - TSideSpots[R, λ, nopt, mopt, q[0], notch, rpat * 10^-3]) * 100,
  (1 - TRadial[R, λ, nopt, mopt, q[0], rmpc, rpat * 10^-3]) * 100}, {rpat, 0, 25.4}, AspectRatio → 1.5,
 AxesLabel → {"ρpat-c (mm)", "Clipping Losses (%)"}, PlotStyle → {Thick, {RGBColor[0.8, 0.1, 0], Thick}}]
```

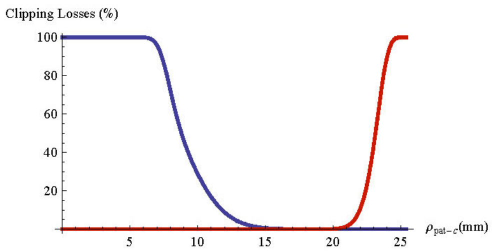


```
PowerGraph =
  Plot[{pout[pp, λp, a, toc, t0, tmpcmirror, tgti, η, R, λ, nopt, mopt, q[0], rmpc, rpat * 10^-3, notch] * 1000,
    pout[pp, λp, a, toc, t0, tmpcmirror, tgti, η, R, λ, n, m, q[0], rmpc, rpat * 10^-3, notch] * 1000},
   {rpat, 0, 25.4}, PlotRange → {100, 165}, AspectRatio → 1.5,
   AxesLabel → {"ρpat-c (mm)", "Output Power (mW)"}, PlotStyle → {Thick, Thick}];

(* Sensitivity to the Pattern Radius in the Initial Configuration and Optimum Configuration *)
(* Purple Line is the Initial Configuration m=4, n=11 *)
(* Blue Line is the Optimum Configuration m=6, n=11 *)

CurrentRadius = ListPlot[
   {{rpat * 10^3, pout[pp, λp, a, toc, t0, tmpcmirror, tgti, η, R, λ, nopt, mopt, q[0], rmpc, rpat, notch] * 1000}},
   PlotStyle → {PointSize[Large]}];
Show[PowerGraph, CurrentRadius]
```

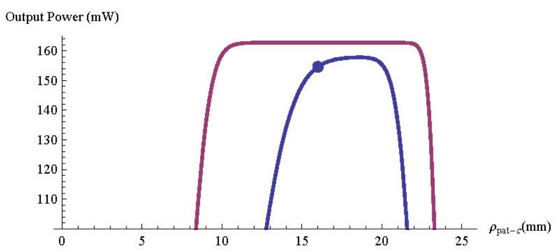

```
(* Simulation of the Optimum Configuration *)
(* Q-Paramter and Spot size for Curved Mirror Spots for Optimum Configuration*)
m = mopt;
n = nopt;

(* Optimum Pattern Radius According to the Graph *)
rpat = 18.5 * 10^-3;
```

```
wf[1] = w[λ, qf1[R, n, m, q[0]]];

For[i = 2, i ≤ n, i++, qf[i] = qfi[R, n, m, q[0], i]; wf[i] = w[λ, qf[i]]]

(* Q-Paramter and Spot size for Curved Mirror Spots *)
For[i = 1, i ≤ n, i++, qc[i] = qci[R, n, m, q[0], i]; wc[i] = w[λ, qc[i]]]

(* Calculation of the Spot Coordinates on MPC mirrors *)
For[i = 1, i ≤ n, i++, θ[i] = (-π i m / n) - π/2; xc[i] = rpat Cos[θ[i]];
 yc[i] = rpat Sin[θ[i]]; xf[i] = rpatf Cos[θ[i]]; yf[i] = rpatf Sin[θ[i]]]
```

```
(* Showing the Numeric Results *)
(* Calculation of Spot Angles in Degrees *)
For[i = 1, i ≤ n, i++,
 θdeg[i] = NumberForm[N[(-(θ[i] + π/2) * 180/π) - (IntegerPart[(-(θ[i] + π/2) * 180/π) / 360] * 360)], 4]]

TableForm[Table[{i, θdeg[i], NumberForm[wc[i] * 10^3, 4], NumberForm[wf[i] * 10^3, 4]}, {i, 1, n}],
 TableHeadings → {{}, {"i     ", "θ(°)   ", "wc(mm) ", "wf(mm)"}}]
```

i	$\theta(°)$	w_c (mm)	w_f (mm)
1	98.18	3.153	1.584
2	196.4	0.9254	1.126
3	294.5	2.895	1.902
4	32.73	1.739	0.5915
5	130.9	2.404	2.067
6	229.1	2.419	0.118
7	327.3	1.72	2.065
8	65.45	2.905	0.606
9	163.6	0.9032	1.896
10	261.8	3.156	1.139
11	0.	0.1802	1.574

```
(* Visulisation of the Results *)

(* Pattern radius on the flat mirror *)
rpatf = rpat Cos[m π / (2 n)];

(* Calculation of the Spot Coordinates on MPC mirrors *)
For[i = 1, i ≤ n, i++, xc[i] = rpat Cos[θ[i]];
 yc[i] = rpat Sin[θ[i]]; xf[i] = rpatf Cos[θ[i]]; yf[i] = rpatf Sin[θ[i]]]


Show[Graphics[Circle[{0, 0}, rmpc, {ArcSin[notch / (2 rmpc)] - π / 2, 2 π - ArcSin[notch / (2 rmpc)] - π / 2}]],
 Graphics[Line[{{-notch / 2, -rmpc * Cos[notch / (2 rmpc)]}, {-notch / 2, 0}, {notch / 2, 0},
    {notch / 2, -rmpc * Cos[notch / (2 rmpc)]}}]], Graphics[{LightGray, Dashed, Circle[{0, 0}, rpat]}],
 Graphics[{Thick, Red, Dashed, Circle[{xc[1], yc[1]}, wc[1] * 3]}], Table[{Beam[xc[i], yc[i], wc[i]]}, {i, 1, n}],
 Graphics[Table[{Red, Dashed, Circle[{xc[i], yc[i]}, wc[i] * 3]}, {i, 2, n - 1}]],
 Graphics[{Thick, Red, Circle[{xc[n], yc[n]}, wc[n] * 3]}],
 Graphics[{LightGray, Dashed, Circle[{2 rmpc + gap, 0}, rpatf]}],
 Graphics[Circle[{2 rmpc + gap, 0}, rmpc, {ArcSin[notch / (2 rmpc)] - π / 2, 2 π - ArcSin[notch / (2 rmpc)] - π / 2}]],
 Graphics[Line[{{2 rmpc + gap - (notch / 2), -rmpc * Cos[notch / (2 rmpc)]}, {2 rmpc + gap - (notch / 2), 0},
    {2 rmpc + gap + notch / 2, 0}, {2 rmpc + gap + (notch / 2), -rmpc * Cos[notch / (2 rmpc)]}}]],
 Graphics[{Thick, Red, Dashed, Circle[{xf[1] + 2 rmpc + gap, yf[1]}, wf[1] * 3]}],
 Table[{Beam[xf[i] + 2 rmpc + gap, yf[i], wf[i]]}, {i, 1, n}],
 Graphics[Table[{Red, Dashed, Circle[{xf[i] + 2 rmpc + gap, yf[i]}, wf[i] * 3]}, {i, 2, n - 1}]],
 Graphics[{Red, Dashed, Circle[{xf[n] + 2 rmpc + gap, yf[n]}, wf[n] * 3]}],
 Graphics[Text[Style["Curved mirror", Large], {0, -rmpc - (gap / 2)}]],
 Graphics[Text[Style["Flat mirror", Large], {2 rmpc + gap, -rmpc - (gap / 2)}]]]
```

```
(* Patterns on the MPC mirrors *)
(* Thick dashed beam is the i=1 case *)
(* Optimum Configuration: m=6, n=11 *)
```

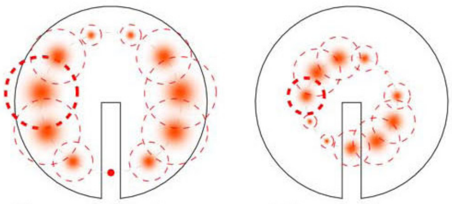

Curved mirror Flat mirror

References

[1] G. J. Tearney, M. E. Brezinski, B. E. Bouma, S. A. Boppart, C. Pitris, J. F. Southern, and J. G. Fujimoto, "*In vivo endoscopic optical biopsy with optical coherence tomography",* Science, Vol. 276, 2037-2039 (1997).

[2] M. Drescher, M. Hentschel, R. Kienberger, U. Heinzmann, and F. Krausz, "*Time resolved atomic inner-shell spectroscopy"*, Nature, Vol. 419, 803-807 (2002).

[3] A. H. Zewail, "*Femtochemistry: recent progress in studies of dynamics and control of reactions and their transition states",* J. Phys. Chem., Vol. 100, 12701 (1996).

[4] C. Spielmann, N. H. Burnett, S. Santania, R. Koppitsch, M. Schnurer, C. Kan, and M. Lenzner, *"Generation of coherent x-rays in the water window using 5-femtosecond laser pulses",* Science, Vol. 278, 661-664 (1997).

[5] Z. Chang, A. Rundquist, H. Wang, M. M. Murnane, and H. C. Kapteyn, *"Generation of coherent soft x rays at 2.7nm using high harmonics",* Phys. Rev. Lett., Vol. 79 (1997).

[6] A. M. Kowalevicz, T. R. Schibli, F. X. Kaertner, and J. G. Fujimoto, *"Ultralow-threshold Kerr-lens mode-locked* $TiAl_2O_3$ *laser"*, Opt. Lett., Vol 27, 2037-2039 (2002).

[7] S. H. Cho, B. E. Bouma, E. P. Ippen, and J. G. Fujimoto, *"Low-repetition-rate high-peak-power Kerr-lens mode-locked* $Ti{:}Al_2O_3$ *laser with a multiple-pass cavity",* Optics Letters, Vol. 24, Issue 6, pp. 417-419 (1999).

[8] A. M. Kowalevicz, A. Sennaroğlu, A. T. Zare and J. G. Fujimoto, *"Design principles of q-preserving multipass-cavity femtosecond lasers"*, Opt. Soc. Am. B/Vol. 23, No. 4 (2006).

[9] A. Sennaroğlu, *"Solid-state Lasres and Applications"*, Ch. 8, p. 321, CRC Press. USA (2007).

[10] D. H. Sutter, G. Steinmeyer, L. Gallmann, N. Matuschak, F. Morier-Genoud, U. Keller, V. Scheuer, G. Angelow, and T. Tschudi,*"Semiconductor saturable-absorber mirror-assisted Kerr-lens mode-locked Ti:Sapphire laser producing pulses in the two cycle regime",* Opt. Lett., Vol. 24, 631-633 (1999).

[11] O. D. Mücke, R. Ell, A. Winter, J. Kim, J. R. Birge, L. Matos, and F. X. Kärtner, *"Self-Referenced 200 MHz Octave-Spanning Ti:Sapphire Laser with 50 Attosecond Carrier-Envelope Phase Jitter"*, Opt. Express, Vol. 13, 5163-5169 (2005).

[12] U. Morgner, F. X. Kärtner, S. H. Cho, Y. Chen, H. A. Haus, J. G. Fujimoto, E. P. Ippen, V. Scheuer, G. Angelow, and T. Tschudi, *"Sub-two-cycle pulses from a Kerr-lens mode-locked Ti:sapphire laser"*, Opt. Lett., Vol. 24, 411-413 (1999) .

[13] H. A. Haus, *“Mode-locking of lasers”,* IEEE J. Sel. Top. Quant. Electron., Vol. 6, 1173-1185 (2000).

[14] P. Weinberger, *"John Kerr and his Effects Found in 1877 and 1878"*, Phil. Mag. Lett., 88 (12): 897–907 (2008).

[15] T. Brabec, Ch. Spielmann, P. F. Curley, and F. Krausz, *“Kerr lens mode-locking”,* Opt. Lett., Vol. 17, Issue 18, pp. 1292-1294 (1992).

[16] J. R. Pierce, “*Theory and Design of Electron Beams”,* Van Nostard (1954).

[17] D. Herriott, H. Kogelnik, and R. Kompfner, *“Off-axis paths in spherical mirror interferometers”,* Appl. Optics 3, 523–26 (1964).

[18] S. H. Cho, B. E. Bouma, E. P. Ippen, and J. G. Fujimoto, *“Low-repetition-rate high-peak-power Kerr-lens mode-locked Ti:Al_2O_3 laser with a multiple-pass cavity”,* Optics Letters, Vol. 24, Issue 6, pp. 417-419 (1999).

[19] A. M. Kowalevicz, A. Sennaroğlu, A. T. Zare and J. G. Fujimoto, *“Design principles of q-preserving multipass-cavity femtosecond lasers”*,Opt.Soc. Am. B/Vol. 23, No. 4 (2006).

[20] A. Yariv, P. Yeh, *“Photonics”*, Sixth Ed., Oxford University Press, pp. 66-67, USA (2007).

[21] A. Yariv, P. Yeh, *“Photonics”*, Sixth Ed., Oxford University Press, p. 84, USA (2007).

[22] J. T. Verdeyen, *“Laser Electronics”*, Third Ed., Prentice Hall Inc., pp. 76, USA (1995).

[23] A. Sennaroğlu and J. G. Fujimoto, *“Design criteria for Herriott-type multi-pass cavities for ultrashort pulse lasers”*, Opt. Express **11**, 1106-1113 (2003).

[24] A. M. Kowalevicz, A. Sennaroğlu, A. T. Zare and J. G. Fujimoto, *“Design principles of q-preserving multipass-cavity femtosecond lasers”*,Opt. Soc. Am., B/Vol. 23, No. 4 (2006).

[25] A. Sennaroğlu, *“Solid-state Lasres and Applications”*, CRC Press, pp. 330-333, USA (2007).

[26] J. T. Verdeyen, *“Laser Electronics”*, Third Ed., Prentice Hall Inc., pp. 68, USA (1995).

[27] A. M. Kowalevicz, A. Sennaroğlu, A. T. Zare and J. G. Fujimoto, *“Design principles of q-preserving multipass-cavity femtosecond lasers”*, Opt. Soc. Am. B/Vol. 23, No. 4 (2006).

[28] Charles A. Poynton, *“Digital Video and HDTV: Algorithms and Interfaces”*, Morgan Kaufmann, pp. 260, 630. ISBN 1558607927 (2003).

[29] A. Sennaroğlu, *“Solid-state Lasres and Applications”*, CRC Press, p. 334, USA (2007).

[30] A. Sennaroğlu, *“Photonics and Laser Engineering: Principles, Devices, and Applications”,* McGraw-Hill Professional, 1st. Edition, ch. 6, (2010).

[31] Jing-yuan Zhang, Jung Y. Huang, H. Wang, K. S. Wong, and G. K. Wong, *“Second-harmonic generation from regeneratively amplified femtosecond laser pulses in BBO and LBO crystals”,* JOSA B, Vol. 15, Issue 1, pp. 200-209 (1998).

[32] A. Yariv, P. Yeh, “Photonics”, Sixth Ed., Oxford University Press, p. 492, USA (2007).